OLD DOMINION UNIVERSITY RESEARCH FOUNDATION

DEPARTMENT OF PHYSICS AND GEOPHYSICAL SCIENCES
SCHOOL OF SCIENCES AND HEALTH PROFESSIONS
OLD DOMINION UNIVERSITY
NORFOLK, VIRGINIA

Technical Report PGSTR-AP77-54

TEMPERATURE AND PRESSURE DEPENDENCE OF DICHLORO-DIFLUOROMETHANE (CF_2Cl_2) ABSORPTION COEFFICIENTS FOR CO_2 WAVEGUIDE LASER RADIATION

By

Charles N. Harward

Progress Report

Prepared for the
National Aeronautics and Space Administration
Langley Research Center
Hampton, Virginia

Under
Research Grant NSG 1197
September 1, 1976 - June 30, 1977
Frank Allario, Technical Monitor
Environmental and Space Sciences Division

August 1977

DEPARTMENT OF PHYSICS AND GEOPHYSICAL SCIENCES
SCHOOL OF SCIENCES AND HEALTH PROFESSIONS
OLD DOMINION UNIVERSITY
NORFOLK, VIRGINIA

Technical Report PGSTR-AP77-54

TEMPERATURE AND PRESSURE DEPENDENCE OF DICHLORODIFLUOROMETHANE (CF_2Cl_2) ABSORPTION COEFFICIENTS FOR CO_2 WAVEGUIDE LASER RADIATION

By

Charles N. Harward

Progress Report

Prepared for the
National Aeronautics and Space Administration
Langley Research Center
Hampton, Virginia 23665

Under
Research Grant NSG 1197
September 1, 1976 - June 30, 1977
Frank Allario, Technical Monitor
Environmental and Space Sciences Division

Submitted by the
Old Dominion University Research Foundation
Norfolk, Virginia 23508

August 1977

TEMPERATURE AND PRESSURE DEPENDENCE OF DICHLORO-DIFLUOROMETHANE (CF_2Cl_2) ABSORPTION COEFFICIENTS FOR CO_2 WAVEGUIDE LASER RADIATION

By

Charles N. Harward[1]

INTRODUCTION

In recent years concern has mounted over the destruction of the stratospheric ozone layer by manmade pollutants. With this concern has come the realization that new techniques must be utilized to accurately measure the concentration of these manmade pollutants so that trends can be unambiguously identified. Infrared heterodyne techniques offer the potential for the accurate determination of the total burden and altitude profile. Peyton, et al. (ref. 10) have previously measured tropospheric ammonia and ozone using heterodyne techniques. Seals and Peyton (ref. 12) proposed the use of these techniques to measure certain of the manmade pollutants. Perhaps the most important of these pollutants is dichloro-difluoromethane or CFM-12. This molecule, which is relatively inert in the lower atmosphere, is photodissociated by ultraviolet radiation in the stratosphere and mesosphere. The atomic chlorine which is a product of this photodissociation catalytically destroys ozone by the pair of reactions

$$Cl + O_3 \rightarrow ClO + O_2 \qquad (1)$$

and

$$ClO + O \rightarrow Cl + O_2 . \qquad (2)$$

---

[1] Research Assistant Professor of Physics and Geophysical Sciences, Old Dominion University, Norfolk, Virginia 23508.

Molina and Rowland (ref. 8) indicated in 1974 that this source of Cl and ClO is so large that ozone is likely to be reduced significantly in the future if the production of CFM-12 is not reduced.

This molecule has previously been detected using ground-based Micelson type Fourier Transform Spectrometers (ref. 2), balloon-borne cryogenic sampling systems (ref. 4), balloon-borne grating spectrometers (ref. 9), and gas chromatography (ref. 6). But these measurements were essentially low resolution techniques. The proposed infrared optical heterodyne measurement offers a much more accurate method of measuring CFM-12 because of its inherent sensitivity, ultrahigh resolution, and specificity. As a prelude to the heterodyne measurement of CFM-12 in the atmosphere, measurements have been performed to determine the pressure and temperature dependence of CFM-12 absorption coefficients for CO_2 waveguide laser radiation. The use of the CO_2 laser was suggested by the measurements made by Schnell and Fischer (ref. 11) of the absorption coefficients of CFM-12 using a spectrophone technique. Their values for the absorption coefficients for CO_2 laser radiation indicated optical heterodyne techniques would have reasonably high sensitivity for CFM-12. However, the Schnell and Fischer (ref. 11) measurements were carried out at a single temperature and pressure, and at the center of low pressure CO_2 laser lines. Since the pressure and temperature in the atmospheric region of interest may vary from 760 to 20 torr and 300° to 215° K, respectively, pressure and temperature measurements were needed. Also, before heterodyne measurements can be performed, the wavelength dependence of the absorption coefficients around possible oscillator lines must be known. This dependence was determined using a technique similar to that used by Menzies (ref. 7) in the CO_2 wavelength guide measurements on ozone.

The absorption coefficients of CFM-12 for CO_2 waveguide laser radiation were found to have no spectral structure within small spectral bandwidths around the CO_2 waveguide laser lines in the $00°1 - (10°0, 02°0)_I$ CO_2 band for pressures above 20 torr. All of the absorption coefficients for the CO_2 laser lines studied are independent of pressure above 100 torr except for the P(36) laser line in the $00°1 - (10°0, 02°0)_I$ CO_2 band. The absorption

coefficients associated with the P(42) line in the same band showed the greatest change with temperature, and it also has the largest value of all the lines studied.

EXPERIMENTAL DETAILS AND RESULTS FOR THE WAVELENGTH DEPENDENCE STUDIES

The radiation source used in this study was a CO_2 waveguide laser that operated in the $00°1 - (10°0, 02°0)_I$ CO_2 band. This laser was designed and built to the same specifications as the one used by Menzies (ref. 7) for the ozone spectroscopy and described by Abrams (ref. 1). The emission bandwidth of the waveguide laser was a function of the total pressure in the waveguide cavity and the ratio of the gases used in the gas mixture. The pressure and mixture ratios used were those that maximized the bandwidth. The optimized bandwidth of the laser decreased monotonically from 595 MHz for the P(26) line down to 133 MHz for the P(46) line. The emission bandwidth for the P(48) line was 195 MHz. This increase over the P(46) line value was the result of the installation of a new grating on the waveguide. The instantaneous line width of the laser was .1 MHz, which was determined by beating the waveguide against a passively stabilized, low pressure CO_2 laser.

The output of the waveguide laser was split into two parts. One part went through an absorption cell (length = 31.75 cm). The other part went through a monochromator, which was used to identify the different laser lines. The infrared radiation passing through the absorption cell was detected by a high-speed Hg-Cd-Te detector. The output from the detector was displayed on an oscilloscope and recorded via photographs.

Figures 1 through 12 are photographs of oscilloscope traces as the waveguide laser was tuned across its emission bandwidth for the P(26) to P(48) laser lines in the $00°1 - (10°0, 02°0)_I$ CO_2 band. The different traces in each photograph are the result of adding various pressures of pure CFM-12 to the absorption

cell. The top trace is always the empty cell case. The CFM-12 pressures are indicated in each figure along with the emission bandwidth of the particular line being studied. The spectral structure on the traces is evident for all of the lines except the P(46) line, where the bandwidth is such that no spectral structure is discernible. Most of the spectral structures have halfwidths which are very much larger than the Doppler halfwidth of 15 MHz. Therefore, the structure must be made up of many individual CFM-12 absorption lines since the laser can resolve .1 MHz. Figures 13 and 14 verify that this is true. These two figures are photographs of the oscilloscope trace as the waveguide laser is tuned across the emission bandwidth for the P(34) line with 77 microns and 10 microns, respectively, of pure CFM-12 in a 10 meter cell. The spectral feature in the center of the laser output in figure 13 looks like a single absorption line, but the halfwidth of 70 MHz is too large for a single Doppler broadened absorption line. In figure 14 both the horizontal and vertical scales have been expanded. The reduced pressure has helped to bring out the individual lines that make up the spectral feature in figure 13. The fine structures on the trace have widths that vary from 15 to 20 MHz. The separation between individual absorption lines is quite small. In fact, there is not a definite point where one line begins and the next line ends. When N_2 gas is added to the CFM-12, in sufficient quantities, the individual lines are broadened so that they blend into one another and form a pseudocontinuum. This is shown in the next set of figures, figures 15 through 26.

Each of these figures is a photograph of the oscilloscope trace of the detector output as the waveguide laser is scanned across its emission bandwidth for various pressures of N_2 added to a pure CFM-12 sample. In each figure the trace (a) is the empty cell case and trace (b) is the pure sample case. All of the other traces are for various partial pressures of N_2 added to the pure sample as indicated in the figure. The spectral structure is smoothed out as the pressure of N_2 is increased.

In fact, there is no spectral structure on any of the CO_2 laser lines studied for N_2 pressures above 20 torr.

Figure 27 shows the experimental absorption coefficient for the P(34) waveguide laser line. This curve was generated by scanning the detector output with a boxcar averager with and without gas in the absorption cell for various pressures of N_2 added to the same CFM-12 sample. From these measurements the absorption coefficient was calculated from a knowledge of the absorbing gas pressure which was .260 torr.

Curve 1 is the absorption coefficient for a pure gas sample. Curves 2 through 6 are the absorption coefficients after N_2 has been added to the cell with total pressures of 2, 4, 8, 16, and 32 torr, respectively. Note that the absorption coefficient is flat for the 32-torr pressure. Although the absorption coefficient has no spectral structure above 32 torr, the value of the absorption coefficient increases to a constant value of 43.5 $(atm\text{-}cm)^{-1}$ for pressures above 100 torr.

EXPERIMENTAL DETAILS AND RESULTS FOR PRESSURE AND TEMPERATURE STUDIES

Since there is no spectral structure within the emission bandwidth of the waveguide laser for all lines for all pressures above 20 torr, the temperature dependence measurements were carried out with the waveguide laser set at the center of the emission line. The chopped output of the waveguide is divided into three parts: one part goes through a monochromator which was used to identify the laser lines; the second part goes through an absorption cell; and the third part passes to a reference detector and is used to monitor changes in the laser output.

The absorption cell could be cooled to stratospheric temperatures and was designed to minimize thermal gradients along the length of the cell. The cell is shown in figure 28. The cell has an inside diameter of 1.59 cm and a length of 31.75 cm. It

is constructed from stainless steel with two coils of 0.635-cm copper tubing silver soldered to the outer cell wall. Vapor from a pressurized LN_2 dewar ran through each of the coils in opposite directions and thus helped to decrease thermal gradients. A 10.16-cm thick covering of styrofoam insulated the cell. An evacuable double window assembly on each end of the cell was used to keep the KCl windows from becoming fogged with condensed water vapor. The wall temperature of the cell was measured by five Chromel Alumel thermocouples attached along the cell walls as indicated in figure 29. The thermal gradient along the cell walls was less than ± 2° C, except at the extreme ends of the wall where it was twice as great.

The gas samples used in these measurements were mixtures of CFM-12 and N_2. The mixtures were premixed in a mix tank for at least 12 hours before they were used in the absorption cell. A heating tape wrapped around the bottom of a mix tank provided for convective mixing of the gases. There was no indication of incomplete mixing in any of the samples used even though a particular mixture was used over periods of weeks.

The mixture ratio used for a given CO_2 laser line was chosen so that the transmission at the highest pressures was no less than 10 percent. The ratio of the mixtures varied from 8.6×10^{-4} for the P(42) CO_2 laser line up to 8.8×10^{-3} for the P(22) CO_2 laser line.

The electronics are shown in figure 29. The chopped outputs from the absorption cell detector and the reference detector were fed into the inputs to a dual channel boxcar averager that was triggered by the reference signal from the chopper. The two inputs were processed and ratioed; then the ratio went to channel 6 on a programmable channel scanner and to a stripchart recorder. The output from an electronic manometer, which measured the absorption cell pressure, went to channel 0 on the channel scanner. The thermocouples mounted to the absorption cell walls were connected to channels 1 through 5. Channel 7 was connected to

an ice bath reference thermocouple. A programmable calculator sequentially scanned each channel, and a digital voltmeter measured the channel output. The calculator recorded the outputs of each channel. These were later processed, and the absorption coefficients were calculated and plotted versus pressure. The absorption coefficients, pressure, and average cell temperature were recorded on cassette tapes for later use.

Figures 30 to 43 show the effects of temperature and pressure on the CFM-12 unnormalized absorption coefficients for the P(22) line through the P(48) CO_2 laser lines of the 00°1 - $(10°0,02°0)_I$ band. All of the absorption coefficients for all of the CO_2 laser lines studied are independent of pressure above 100 torr except for the absorption coefficient for P(36), which is pressure independent above 400 torr. Table 1 presents the room temperature absorption coefficient for each of the laser lines studied. The tabulated values are averages of the absorption coefficients for pressure above 100 torr, except for the value for P(36) where the average was taken for pressures above 400 torr. Values of the absorption coefficient for P(44), P(46), and P(48) were obtained for the first time. Comparisons are also made with the values published by Schnell and Fischer (ref. 11) and the values of Goldman, et al. (ref. 3). The measurements of Schnell and Fischer (ref. 11) were carried out using a low-pressure CO_2 laser as the radiation source for a spectrophone detector. These measurements were carried out at a single pressure and temperature. The absorption coefficient values for all the laser lines studied are within 17 percent of the Schnell and Fischer values.

The values published by Goldman, et al. (ref. 3) were determined from a statistical band model fit to low resolution spectra of CFM-12. The agreement with the present determination is quite good in the middle of the R branch of the CFM-12 band. The disagreement around P(40) and P(42) is expected because these two lines are in a spectral region where the shape of the CFM-12

Table 1. Comparison of room temperature absorption coefficients of Freon-12 for selected CO_2 waveguide laser lines in the 00°1 - $(10°0,02°0)_I$ CO_2 band. The absorption coefficients are expressed in units of $(atm\text{-}cm)^{-1}$ NPT.

P(J)	Wavenumber (cm^{-1})	Present $(atm\text{-}cm)^{-1}$	Schnell et al. (ref. 11) $(atm\text{-}cm)^{-1}$	Percent Error	Goldman et al. (ref. 3) $(atm\text{-}cm)^{-1}$	Percent Error
22	942.38407	0.5	0.5	0	1.0	100.0
24	940.54883	1.4	1.2	14.3	3.0	185.0
26	938.68899	3.5	3.1	11.4	5.0	42.9
28	936.80447	8.8	8.3	6.7	11.0	23.6
30	934.89522	18.1	17.4	3.9	19.5	7.7
32	932.96115	31.5	27.0	14.3	32.0	1.6
34	931.00217	43.5	36.0	17.2	41.3	5.1
36	929.01820	45.7	42.0	8.1	42.0	8.1
38	927.00914	40.9	38.0	7.1	37.5	8.3
40	924.97487	29.9	29.0	3.0	38.0	27.1
42	922.91528	94.7	92.0	2.9	48.5	48.9
44	920.83025	53.7	-	-	49.0	8.8
46	918.71966	36.0	-	-	38.0	5.4
48	916.58300	33.8	-	-	37.0	9.5

band is changing rapidly because of the presence of intense Q branches (ref. 3). Low resolution spectra cannot follow these changes accurately. It is somewhat surprising that the laser measurements agree as well as they do with the low resolution values. This points to the fact that the spacing between different CFM-12 absorption lines is very small as was pointed out in reference to figures 13 and 14. The pressure-broadened absorption lines form a pseudocontinuum so that low resolution and high resolution absorption coefficient determinations yield the same results.

The average absorption coefficients were normalized to NPT and were fitted with a straight line of the form $K = mT + B$ using the method of least squares. The slope and the y-intercept reported are the result of a fit to at least eight points. The slope m and y-intercept B are tabulated in table 2 along with the standard deviation and ratio of standard deviation to the midpoint value of the absorption coefficient. All of the ratios are less than seven percent, while most are less than three percent. The author is not aware of any previously published values that can be compared with the present work.

SUMMARY AND CONCLUSIONS

The spectral profiles of the absorption of CFM-12 around selected CO_2 waveguide laser lines have been presented under a resolution better than .1 MHz with the spectral scans having a bandwidth of $\leq$ 595 MHz. Spectral structure with a width on the order of 15 to 20 MHz was resolved, and the data reveal that the spacing between adjacent absorption lines is very small. This small spacing leads to a pseudocontinuum for pressures above 20 torr and to a pressure independent absorption coefficient within the emission bandwidth of the laser for pressures above 100 torr, except for the absorption coefficient associated with the P(36) CO_2 laser line which shows a pressure dependence up to 400 torr. The room temperature absorption coefficients of CFM-12 at the center of all of the CO_2 laser lines from P(22) to P(42) of the $00°1 - (10°0,02°0)_I$ band were

Table 2. Linear coefficients for linear least squares fit of the Freon-12 absorption coefficients versus temperature. The relative standard deviation is the ratio of the standard deviation divided by the average absorption coefficient in the temperature range studied.

P(J)	B	M	Sigma	Relative Sigma (Percent)
22	-1.0753	0.00550	0.028	7.94
24	-2.7310	0.01420	0.071	7.52
26	-5.5877	0.03115	0.063	2.53
28	-10.6399	0.06675	0.136	2.05
30	-8.9596	0.09225	0.355	2.38
32	7.7946	0.08078	1.624	5.66
34	43.1024	0.00143	1.023	2.35
36	92.1301	-0.15852	1.539	3.01
38	78.2191	-0.12725	1.204	2.66
40	36.0697	-0.02117	0.397	1.30
42	303.3162	-0.71208	2.199	1.85
44	31.3165	0.07633	0.347	0.68
46	44.0869	-0.02761	0.588	1.59
48	70.9444	-0.12675	0.534	1.40

determined and compared with previously published results. Values for the CFM-12 absorption coefficient for P(44), P(46), and P(48) were presented for the first time. The temperature dependence of the CFM-12 absorption coefficients for all of the CO_2 laser lines from P(22) to P(48) of the 00°1 - $(10°0,02°0)_I$ band have been determined for the first time and the normalized absorption coefficients were fitted with a straight line by the linear least squares method.

Of the CO_2 laser lines studied, the one that would be best suited for use as a local oscillator in an optical heterodyne experiment is P(42) because of the large value of the absorption coefficient for this laser line. The large increase in the absorption coefficient with respect to temperature further increases the sensitivity at higher altitudes for this laser line.

Although the P(42) laser line will have high sensitivity for heterodyne detection of CFM-12, there are other positions in the 10.8-micron band that need to be investigated. Goldman et al. (ref. 3) reported three strongly absorbing Q branches associated with the different isotopic combinations of Cl for the zero vibrational band and also two Q branches associated with the $\nu_6 + \nu_2 - \nu_2$ and $\nu_6 + \nu_5 - \nu_5$ hot bands in the region around the P(42) laser line.* The most strongly absorbing region according to the work of Goldman et. al (ref. 3) is around 923.1 cm^{-1} which is very near the R(12) line of the 00°1 - $(10°0,02°0)_I$ $C^{13}O_2^{16}$ laser. Therefore, the absorption coefficient of CFM-12 for this laser line should be determined. In fact, if a tunable diode laser were available, the region around these Q branches should be investigated to determine the optimum position for the local oscillator for the heterodyne detection of CFM-12; a position in which the spacing between the individual CFM-12 lines is large enough for spectral structure to appear for the higher pressures.

---

* Hinkley et al. (ref. 5) report a value of 275 $(atm\text{-}cm)^{-1}$ at 921 cm^{-1}.

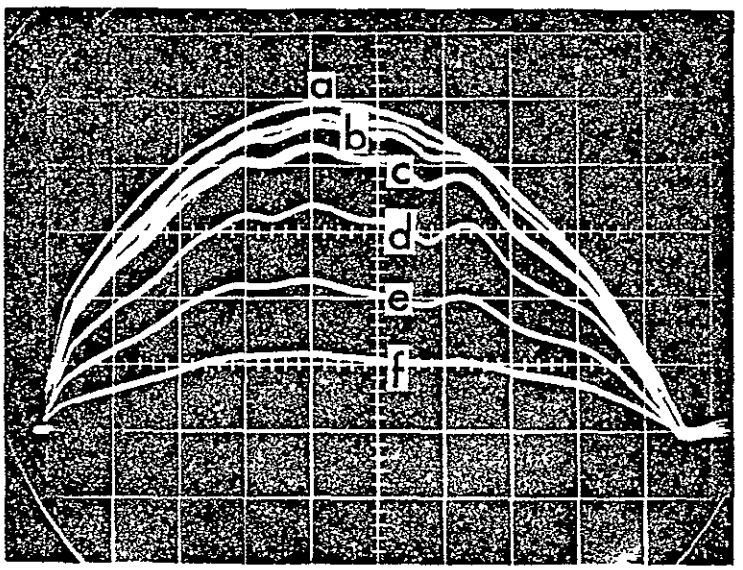

Figure 1. Photograph of oscilloscope trace of the detector output for the P(26) waveguide laser line of the $00°1 - (10°0, 02°0)_I$ CO_2 band with a total band width of 595 MHz for various pressures of pure CFM-12 in the cell: a) empty cell, b) .384 torr, c) .719 torr, d and e) 1.40 torr, f) 3.43 torr, g) 6.7 torr, and f) 12.4 torr.

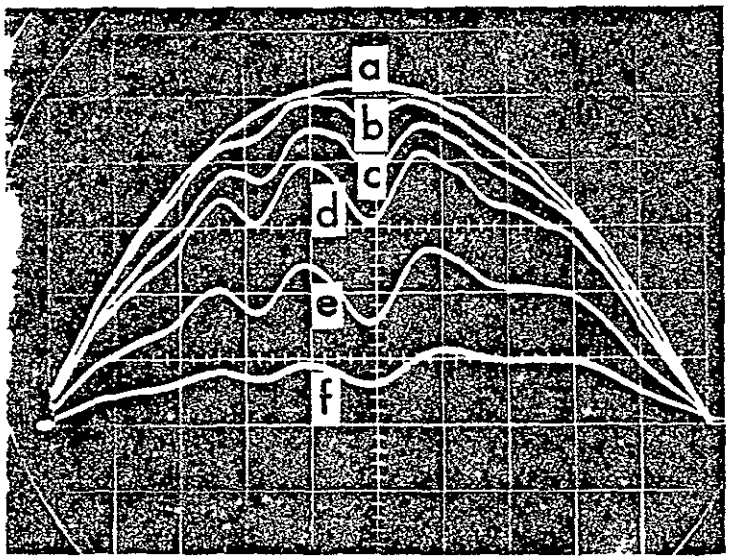

Figure 2. Photograph of oscilloscope trace of the detector output for the P(28) waveguide laser line of the $00^{\circ}1 - (10^{\circ}0, 02^{\circ}0)_{I}$ CO_2 band with a total bandwidth of 545 MHz for various pressures of pure CFM-12 in the cell: a) empty cell, b) .235 torr, c) .516 torr, d) .966 torr, e) 2.48 torr, and f) 5.04 torr.

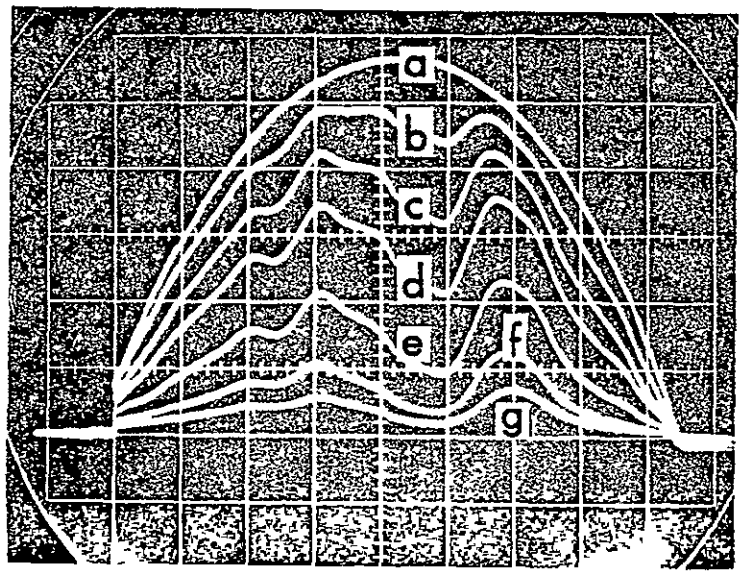

Figure 3. Photograph of oscilloscope trace of the detector output for the P(30) waveguide laser line of the $00^{\circ}1 - (10^{\circ}0, 02^{\circ}0)_{I}$ CO_2 band with a total bandwidth of 530 MHz for various pressures of pure CFM-12 in the cell: a) empty cell, b) .246 torr, c) .536 torr, d) .910 torr, e) 1.75 torr, f) 2.81 torr, and g) 3.75 torr.

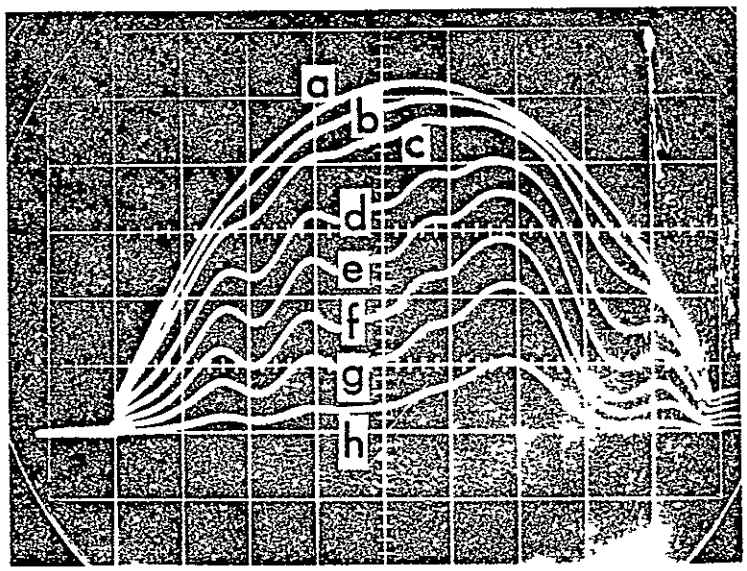

Figure 4. Photograph of oscilloscope trace of the detector output for the P(32) waveguide laser line of the 00°1 - (10°0, 02°0)$_I$ CO_2 band with a total bandwidth of 476 MHz for various pressures of pure CFM-12 in the cell: a) empty cell, b) .100 torr, c) .202 torr, d) .418 torr, e) .659 torr, f) 1.04 torr, g) 1.47 torr, and h) 2.47 torr.

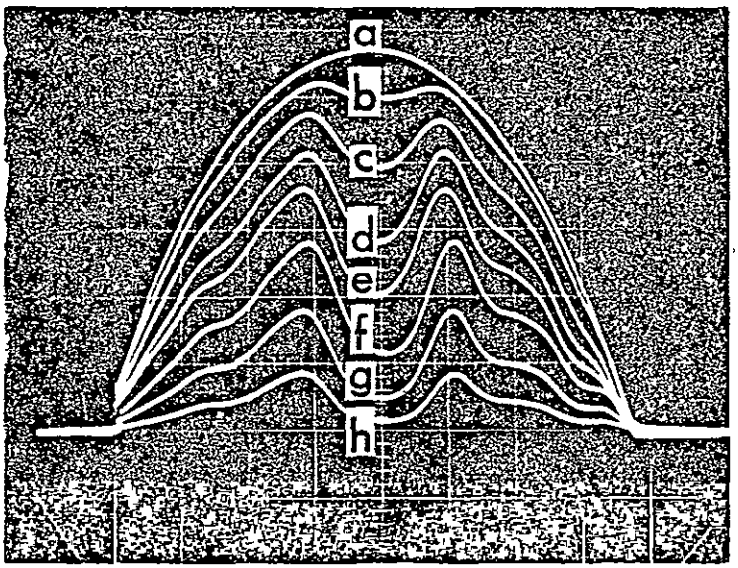

Figure 5. Photograph of oscilloscope trace of the detector output for the P(34) waveguide laser line of the $00^{\circ}1 - (10^{\circ}0, 02^{\circ}0)_{I}$ CO_2 band with a total bandwidth of 421 MHz for various pressures of pure CFM-12 in the cell: a) empty cell, b) .115 torr, c) .220 torr, d) .364 torr, e) .504 torr, f) .781 torr, g) 1.22 torr, and h) 1.86 torr.

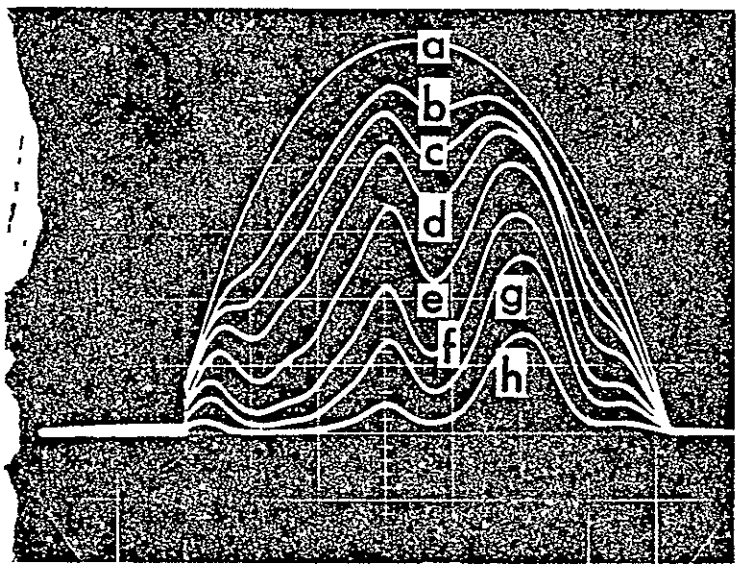

Figure 6. Photograph of oscilloscope trace of the detector output for the P(36) waveguide laser line of the $00^{\circ}1 - (10^{\circ}0, 02^{\circ}0)_{I}$ CO_2 band with a total bandwidth of 394 MHz for various pressures of pure CFM-12 in the cell: a) empty cell, b) .114 torr, c) .166 torr, d) .227 torr, e) .340 torr, f) .559 torr, g) .752 torr, and h) 1.27 torr.

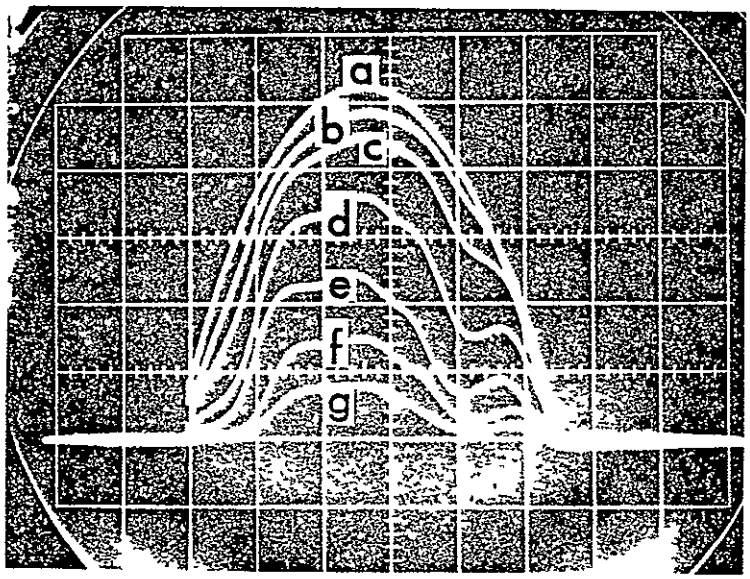

Figure 7. Photograph of oscilloscope trace of the detector output for the P(38) waveguide laser line of the $00°1 - (10°0, 02°0)_I$ CO_2 band with a total bandwidth of 295 MHz for various pressures of pure CFM-12 in the cell: a) empty cell, b) .103 torr, c) .210 torr, d) .514 torr, e) .939 torr, f) 1.52 torr, and g) 2.23 torr.

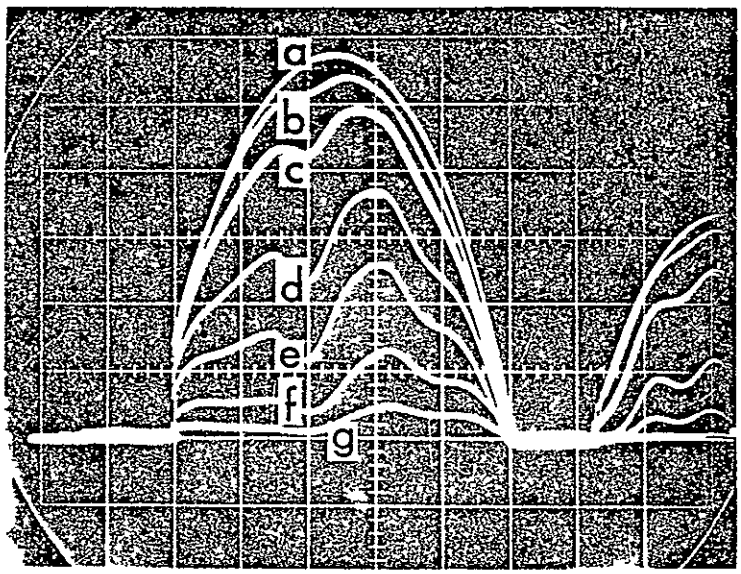

Figure 8. Photograph of oscilloscope trace of the detector output for the P(40) waveguide laser line of the $00^{\circ}1 - (10^{\circ}0, 02^{\circ}0)_{I}$ CO_2 band with a total bandwidth of 262 MHz for various pressures of pure CFM-12 in the cell: a) empty cell, b) .094 torr, c) .182 torr, d) .507 torr, e) .898 torr, f) 1.60 torr, and g) 2.49 torr.

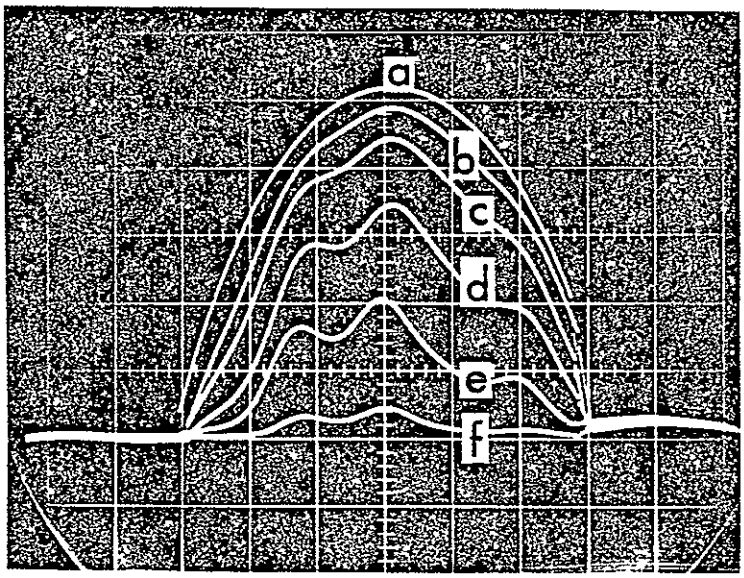

Figure 9. Photograph of oscilloscope trace of the detector output for the P(42) waveguide laser line of the 00°1 - (10°0, 02°0)$_I$ CO_2 band with a total bandwidth of 273 MHz for various pressures of pure CFM-12 in the cell: a) empty cell, b) .060 torr, c) .136 torr, d) .265 torr, e) .454 torr, and f) 1.031 torr.

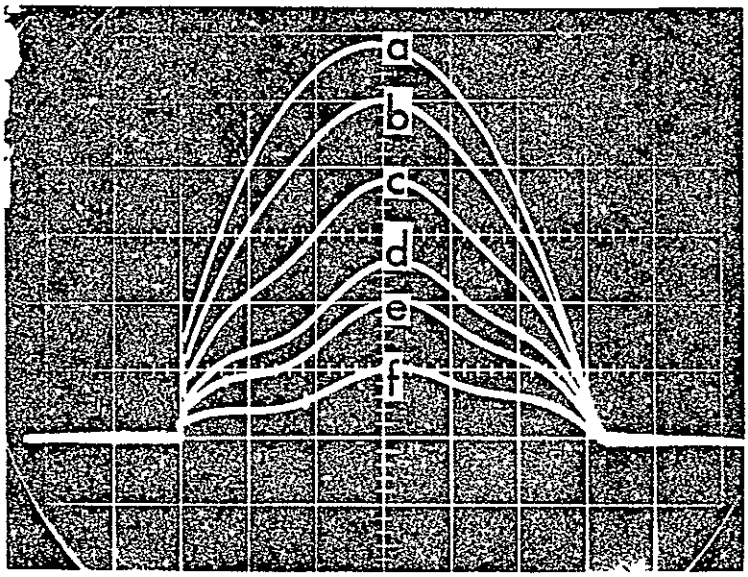

Figure 10. Photograph of oscilloscope trace of the detector output for the P(44) waveguide laser line of the $00^{\circ}1 - (10^{\circ}0, 02^{\circ}0)_{I}$ CO_2 band with a total bandwidth of 159 MHz for various pressures of pure CFM-12 in the cell: a) empty cell, b) .150 torr, c) .294 torr, d) .653 torr, e) .516 torr, and f) 1.037 torr.

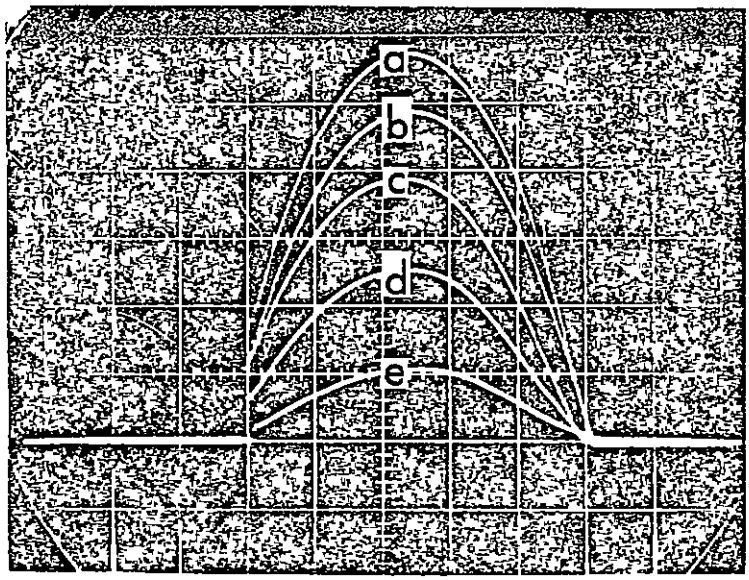

Figure 11. Photograph of oscilloscope trace of the detector output for the P(46) waveguide laser line of the $00°1 - (10°0, 02°0)_I$ CO_2 band with a total bandwidth of 133 MHz for various pressures of pure CFM-12 in the cell: a) empty cell, b) .207 torr, c) .475 torr, d) .950 torr, and e) 1.80 torr.

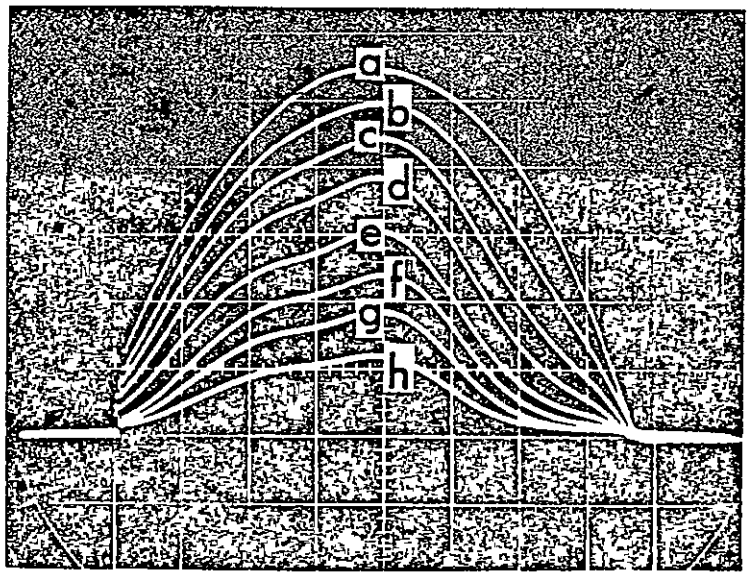

Figure 12. Photograph of oscilloscope trace of the detector output for the P(48) waveguide laser line of the $00^{\circ}1 - (10^{\circ}0, 02^{\circ}0)_{I}$ CO_2 band with a total bandwidth of 195 MHz for various pressures of pure CFM-12 in the cell: a) empty cell, b) .186 torr, c) .350 torr, d) .506 torr, e) .765 torr, f) 1.00 torr, g) 1.26 torr, and h) 1.70 torr.

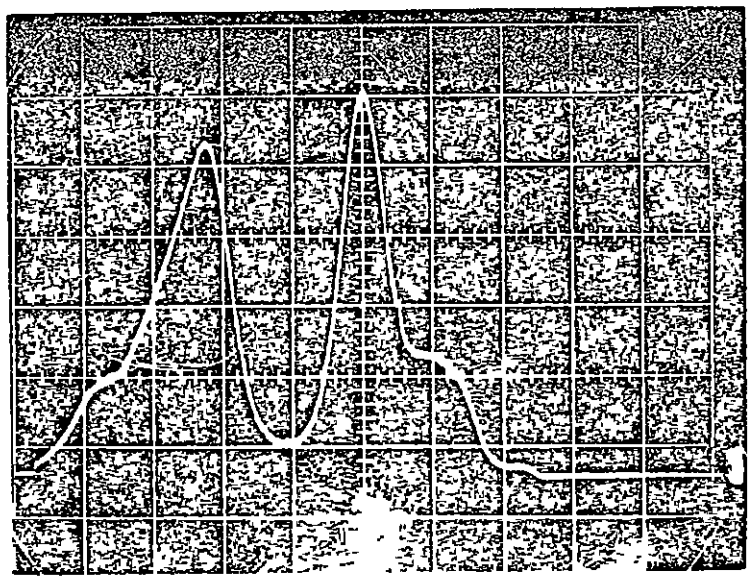

Figure 13. Photograph of oscilloscope trace of the detector output for the P(34) waveguide laser line of the 00°1 - (10°0, 02°0)$_I$ CO_2 band with a pressure of 77μ in a 10 m absorption cell. The half-width of the spectral feature in the center of the trace is approximately 70 MHz.

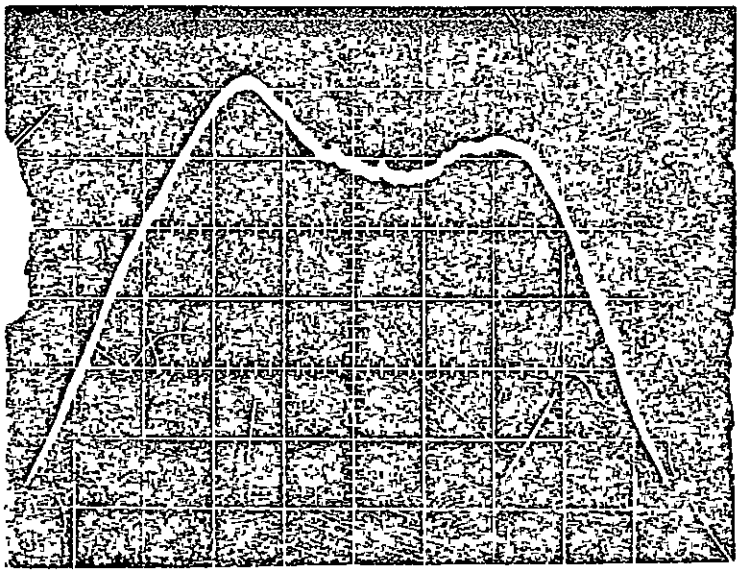

Figure 14. Same as figure 12 except both horizontal and vertical scales have been expanded and the pressure has been reduced to 10μ. Note the fine spectral structure with widths of 15 to 20 MHz.

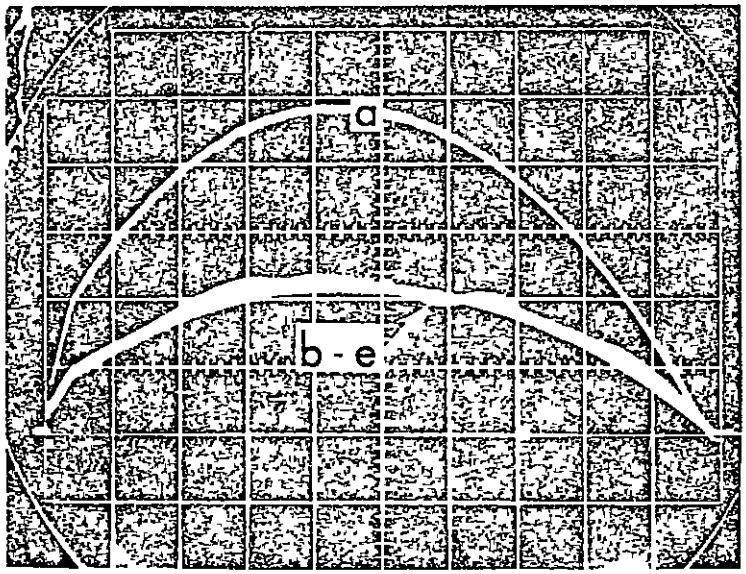

Figure 15. Photograph of oscilloscope trace of the output of a CO_2 waveguide laser operating on the P(26) line in the $00^{\circ}1 - (10^{\circ}0, 02^{\circ}0)_I$ CO_2 band with various pressures of N_2 added to a 6.24 torr pure sample of CFM-12. The total emission bandwidth is 595 MHz: a) empty cell, b) 6.24 torr of pure CFM-12, c) 12.3 torr total pressure, d) 25.8 torr total pressure, and e) 47.3 torr total pressure. Note the lack of spectral structure for pressures above 25 torr.

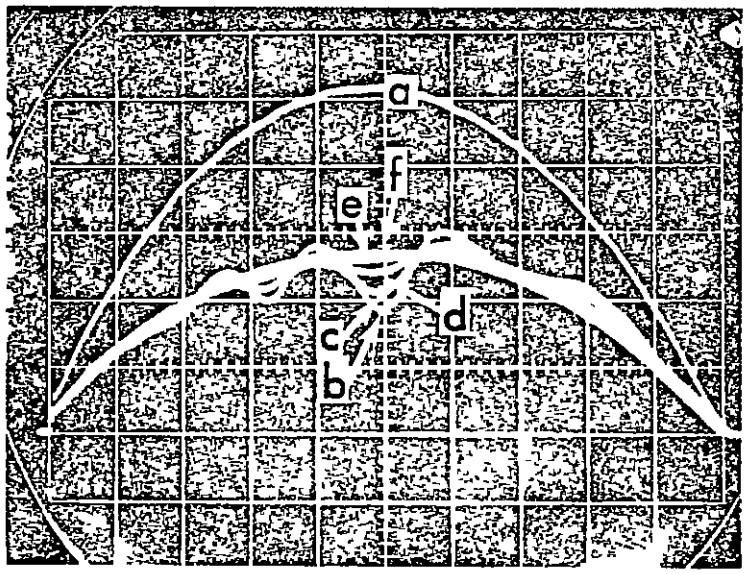

Figure 16. Photograph of oscilloscope trace of the output of a CO_2 waveguide laser operating on the P(28) line in the 00°1 - (10°0, 02°0)$_I$ CO_2 band with various pressures of N_2 added to a 1.93 torr pure sample of CFM-12. The total emission bandwidth is 545 MHz: a) empty cell, b) 1.93 torr pure CFM-12, c) 4.1 torr total pressure, d) 8.17 torr total pressure, e) 17.01 torr total pressure, and f) 36.2 torr total pressure.

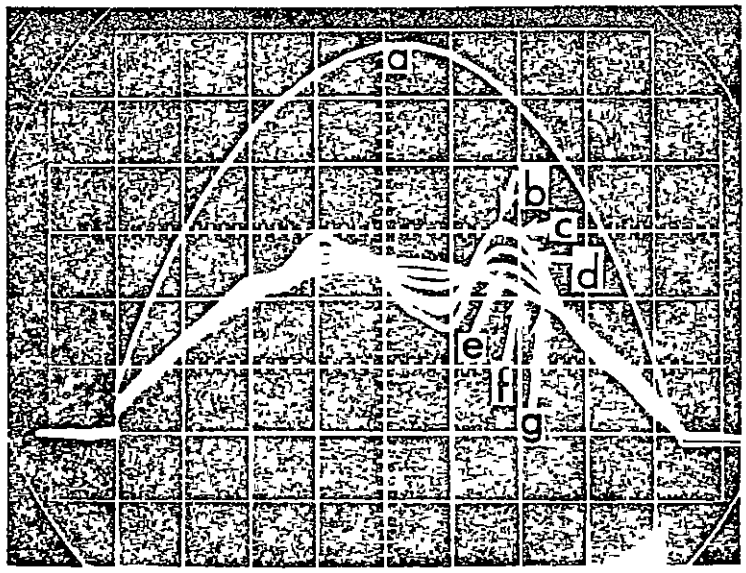

Figure 17. Photograph of oscilloscope trace of the output of a CO_2 waveguide laser operating on the P(30) line in the 00°1 - (10°0, 02°0)$_I$ CO_2 band with various pressures of N_2 added to a 1.205 torr pure sample of CFM-12. The total emission bandwidth is 530 MHz: a) empty cell, b) .205 torr pure CFM-12, c) 2.22 torr total pressure, d) 4.26 torr total pressure, e) 8.4 torr total pressure, f) 17.3 torr total pressure, and g) 43.5 torr total pressure.

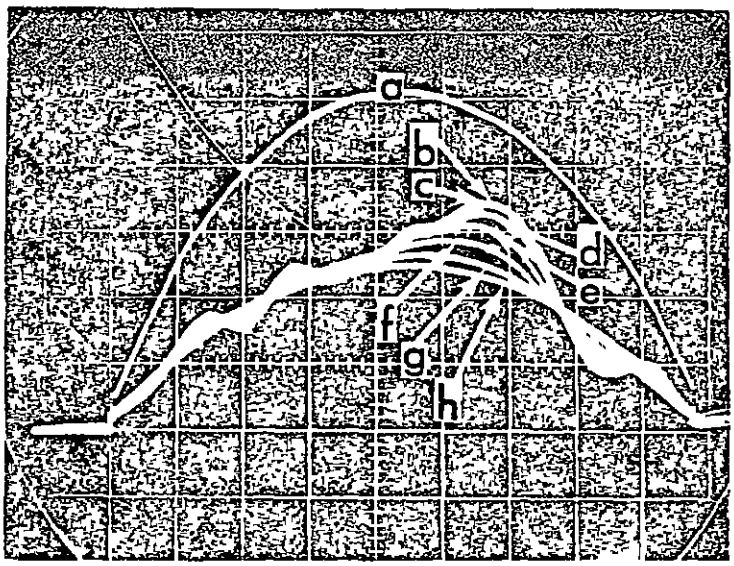

Figure 18. —Photograph of oscilloscope trace of the output of a CO_2 waveguide laser operating on the P(32) line in the $00°1 - (10°0, 02°0)_I$ CO_2 band with various pressures of N_2 added to a .690 torr of pure sample of CFM-12. The total emission bandwidth is 476 MHz: a) empty cell, b) .690 torr of pure CFM-12, c) 1.16 torr total pressure, d) 2.11 torr total pressure, e) 4.32 torr total pressure, f) 8.30 torr total pressure, g) 16.5 torr total pressure, and h) 38.2 torr total pressure.

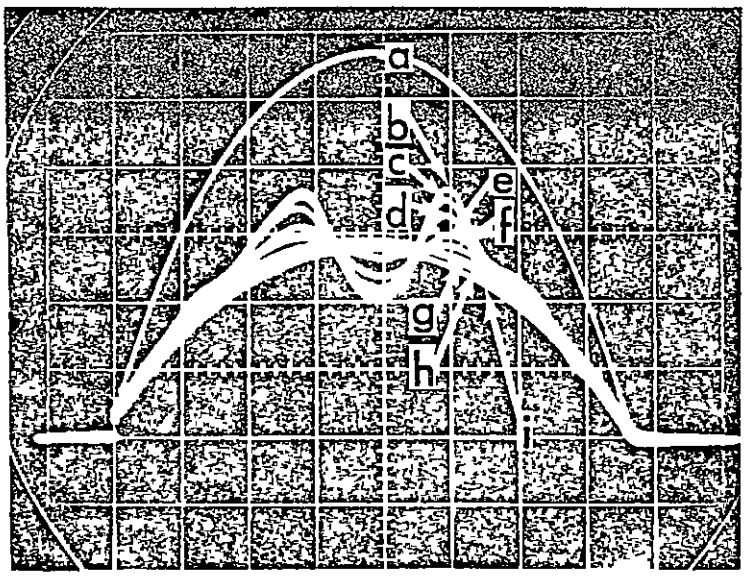

Figure 19. —Photograph of oscilloscope trace of the output of a CO_2 waveguide laser operating on the P(34) line in the 00°1 - (10°0, 02°0)$_I$ CO_2 band with various pressures of N_2 added to a .513 torr of pure sample of CFM-12. The total emission bandwidth is 421 MHz: a) empty cell, b) .513 torr of pure CFM-12, c) 1.073 torr total pressure, d) 2.12 torr total pressure, e) 4.18 torr total pressure, f) 8.02 torr total pressure, g) 16.7 torr total pressure, h) 33.2 torr total pressure, and i) 62.3 torr total pressure.

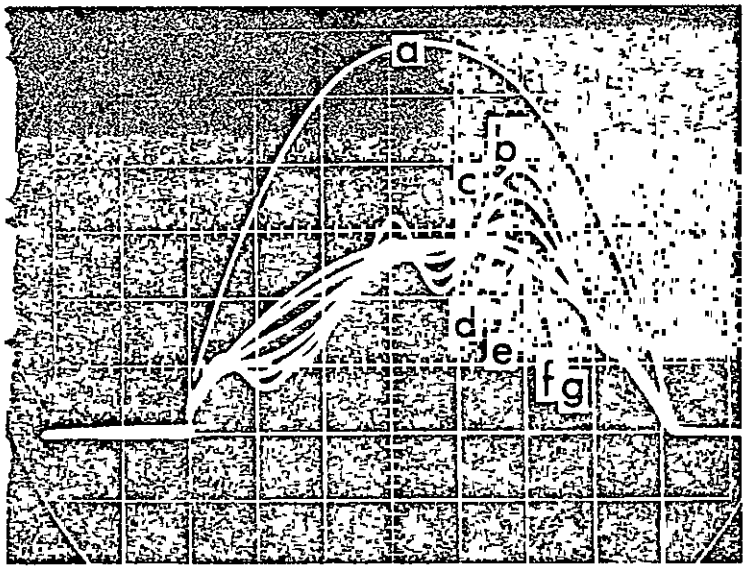

Figure 20. Photograph of oscilloscope trace of the output of a CO_2 waveguide laser operating on the P(36) line in the 00°1 - (10°0, 02°0)$_I$ CO_2 band with various pressures of N_2 added to a .362 torr of pure sample of CFM-12. The total emission bandwidth is 394 MHz: a) empty cell, b) .362 torr of pure CFM-12, c) 2.00 torr total pressure, d) 4.92 torr total pressure, e) 10.49 torr total pressure, f) 20.5 torr total pressure, and g) 42 torr total pressure.

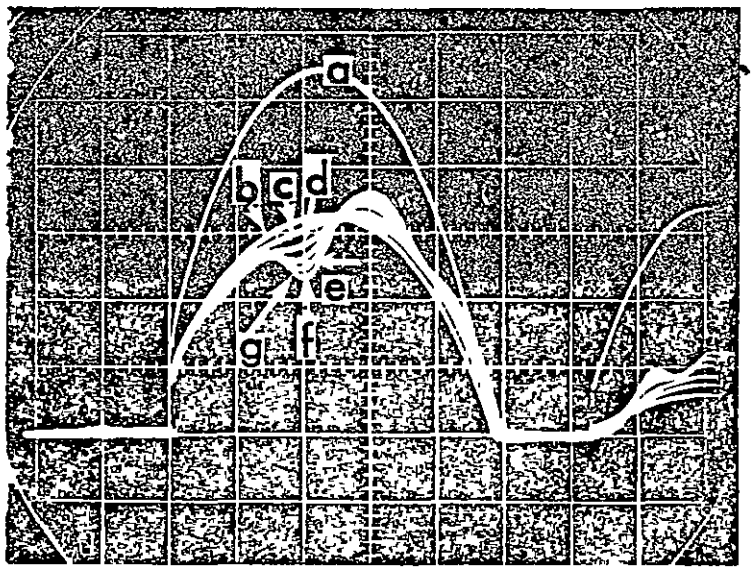

Figure 21. Photograph of oscilloscope trace of the output of a CO_2 waveguide laser operating on the P(38) line in the 00°1 - (10°0, 02°0)$_I$ CO_2 band with various pressures of N_2 added to a .922 torr of pure sample of CFM-12. The total emission bandwidth is 297 MHz: a) empty cell, b) .922 torr of pure CFM-12, c) 2.08 torr total pressure, d) 4.61 torr total pressure, e) 8.55 torr total pressure, f) 16.6 torr total pressure, and g) 33.8 torr total pressure.

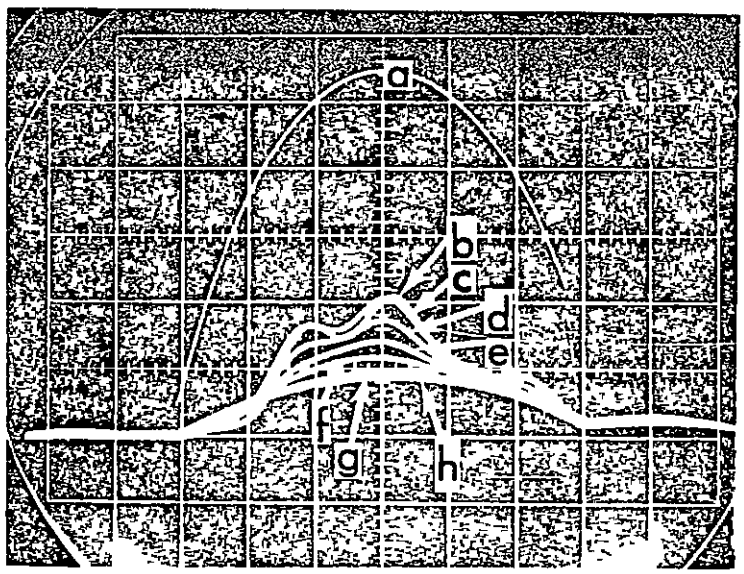

Figure 22. Photograph of oscilloscope trace of the output of a CO_2 waveguide laser operating on the P(40) line in the 00°1 - (10°0, 02°0)$_I$ CO_2 band with various pressures of N_2 added to a .449 torr of pure sample of CFM-12. The total emission bandwidth is 262 MHz: a) empty cell, b) .449 torr of pure CFM-12, c) 1.142 torr total pressure, d) 1.72 torr total pressure, e) 2.09 torr total pressure, f) 4.22 torr total pressure, g) 8.32 torr total pressure, and h) 21.2 torr total pressure.

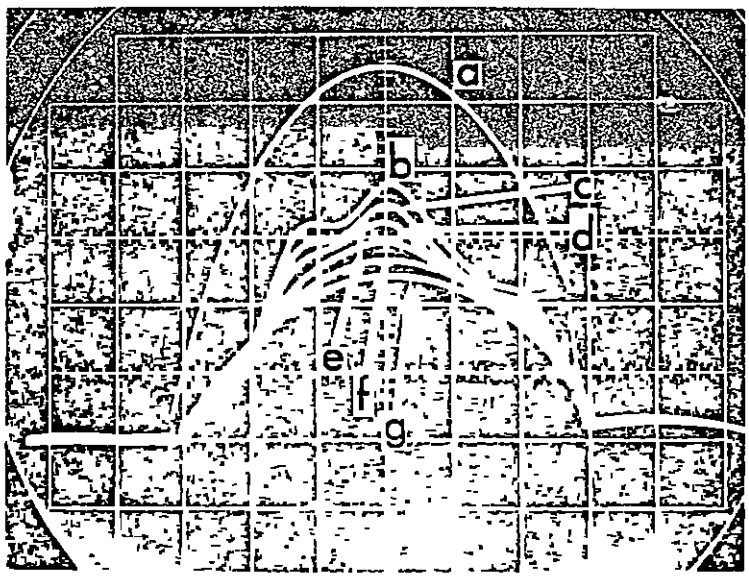

Figure 23. Photograph of oscilloscope trace of the output of a CO_2 waveguide laser operating on the P(42) line in the 00°1 - (10°0, 02°0)$_I$ CO_2 band with various pressures of N_2 added to a .245 torr of pure sample of CFM-12. The total emission bandwidth is 273 MHz: a) empty cell, b) .245 torr of pure CFM-12, c) 1.023 torr total pressure, d) 2.11 torr total pressure, e) 4.63 torr total pressure, f) 10.55 torr total pressure, and g) 21.2 torr total pressure.

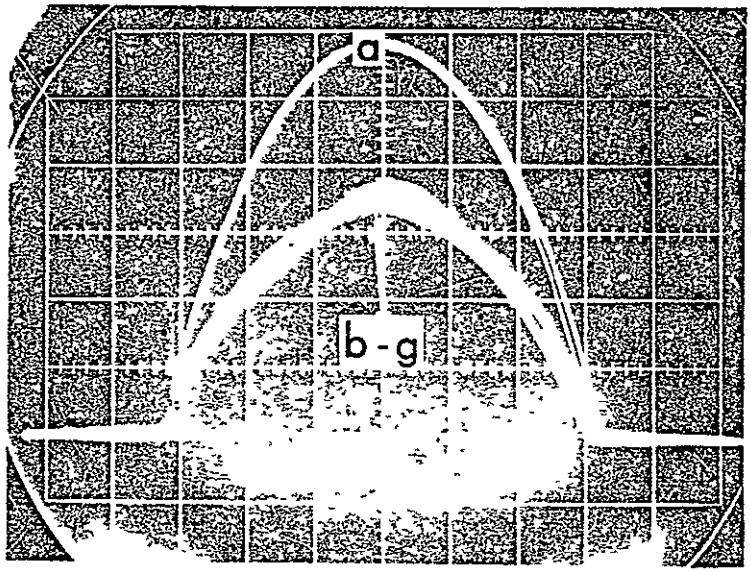

Figure 24. —Photograph of oscilloscope trace of the output of a CO_2 waveguide laser operating on the P(44) line in the 00°1 - (10°0, 02°0)$_I$ CO_2 band with various pressures of N_2 added to a .296 torr of pure sample of CFM-12. The total emission bandwidth is 159 MHz: a) empty cell, b) .296 torr of pure CFM-12, c) 1.087 torr total pressure, d) 2.25 torr total pressure, e) 4.14 torr total pressure, f) 8.19 torr total pressure, and g) 16.94 torr total pressure.

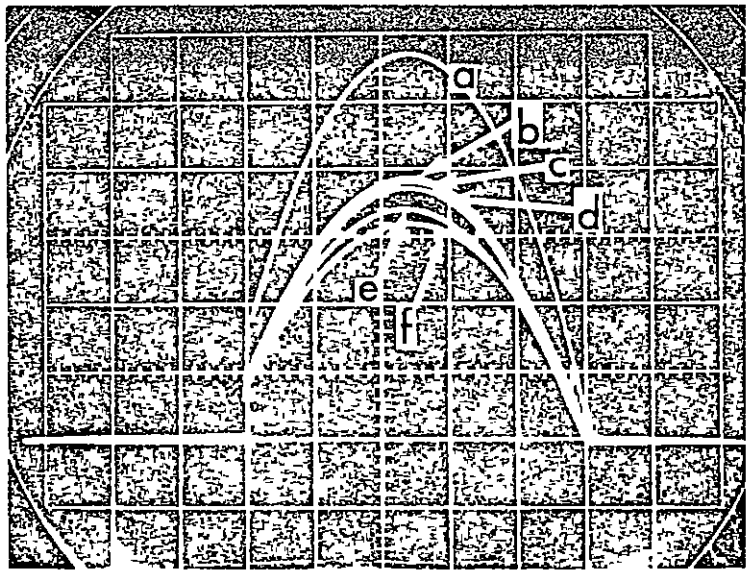

Figure 25. Photograph of oscilloscope trace of the output of a CO_2 waveguide laser operating on the P(46) line in the 00°1 - (10°0, 02°0)$_I$ CO_2 band with various pressures of N_2 added to a .482 torr of pure sample of CFM-12. The total emission bandwidth is 133 MHz: a) empty cell, b) .482 torr of pure CFM-12, c) 1.53 torr total pressure, d) 3.12 torr total pressure, e) 8.16 torr total pressure, and f) 16.3 torr total pressure.

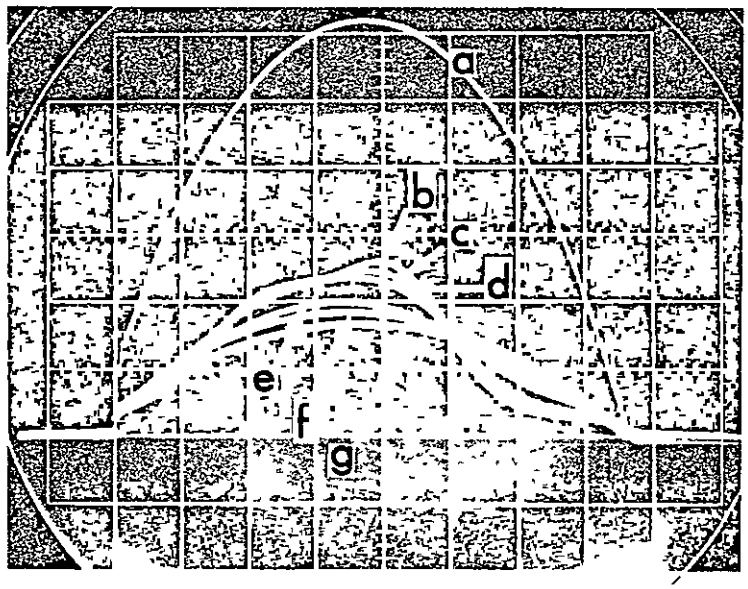

Figure 26. Photograph of oscilloscope trace of the output of a CO_2 waveguide laser operating on the P(48) line in the 00°1 - (10°0, 02°0)$_I$ CO_2 band with various pressures of N_2 added to a 1.01 torr of pure sample of CFM-12. The total emission bandwidth is 195 MHz: a) empty cell, b) 1.01 torr of pure CFM-12, c) 2.12 torr total pressure, d) 4.19 torr total pressure, e) 8.32 torr total pressure, f) 18.07 torr total pressure, and g) 110.2 torr total pressure.

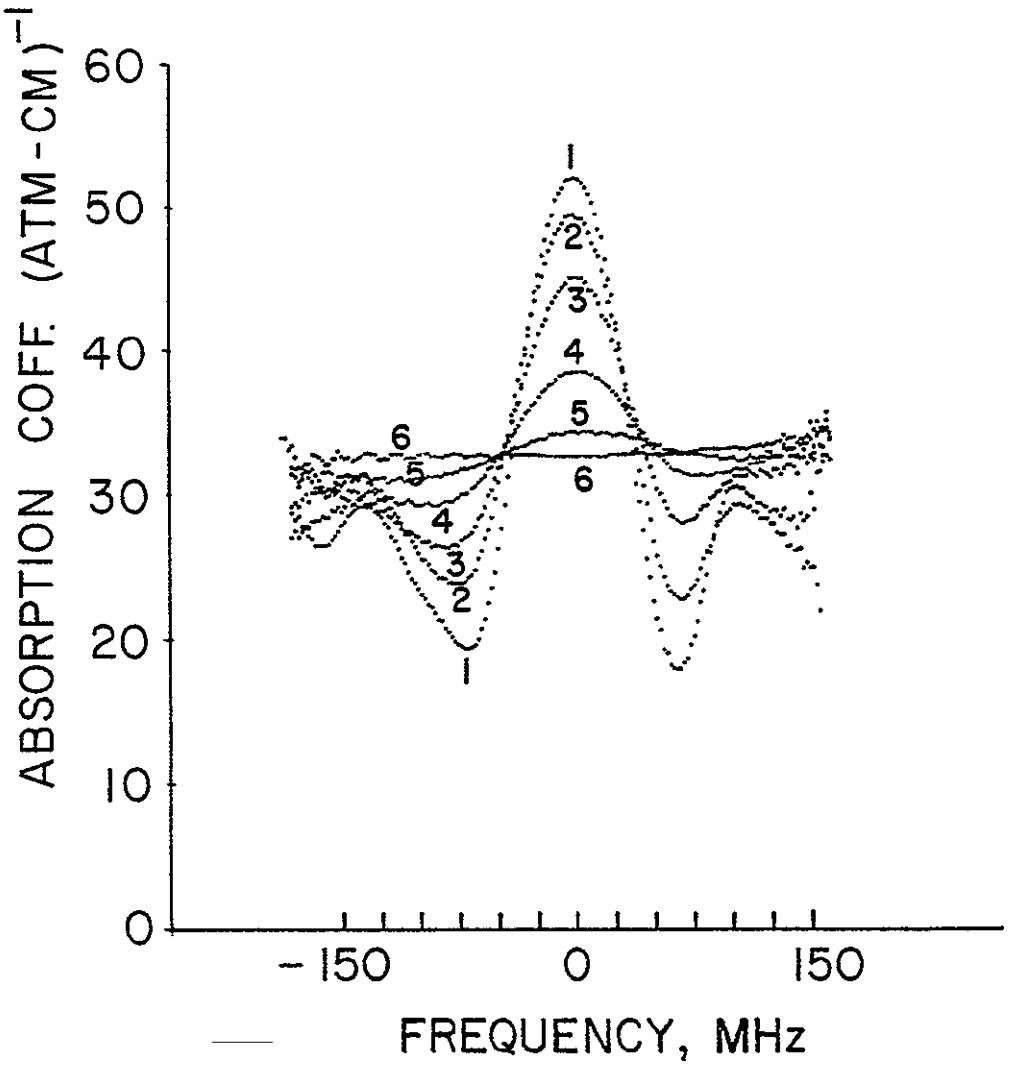

Figure 27. Foreign gas pressure dependence of CFM-12 for the P(34) line of CO_2 waveguide laser line. The absorption coefficient of CFM-12 was determined by scanning a boxcar averager over the output of the waveguide laser as the laser was repeatedly scanned across the P(34) emission line. Curve 1 is the absorption coefficient for .260 torr of pure CFM-12. Curves 2 through 6 are the absorption coefficient of the .260 torr CFM-12 sample with 2, 4, 8, 16 and 32 torr of N_2 added to it. Note the spectral structure for the pure low pressure sample and the lack of spectral structure for the 32 torr N_2 broadened sample.

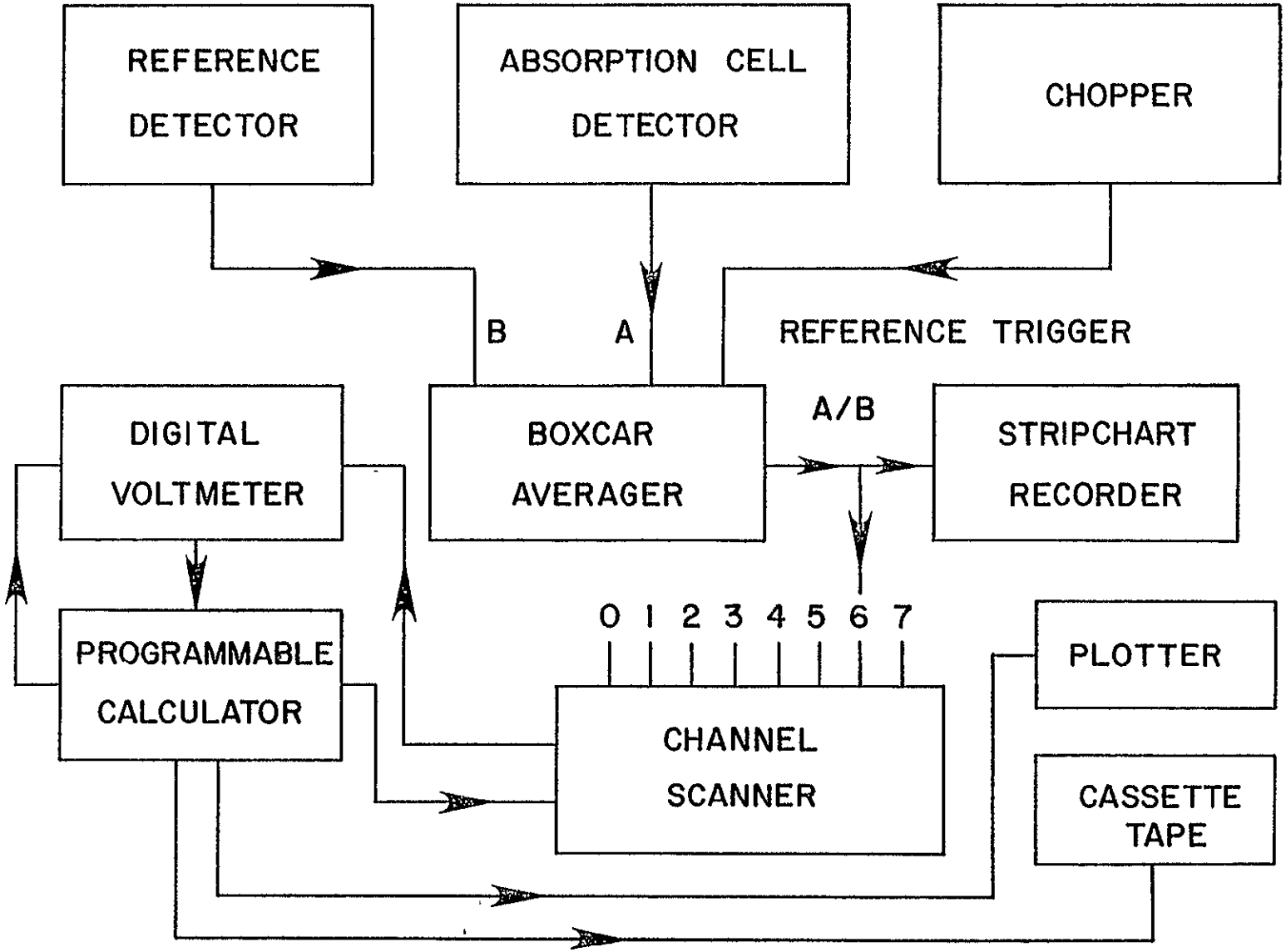

Figure 28. Absorption cell. The absorption cell was 31.75 cm in length constructed from stainless steel. Two coils of copper tubing were wrapped around the cell wall allowing vapors from a pressurized LN_2 dewar to flow in opposite directions along the length of the cell to minimize thermal gradients. The evacuable double window assemblies were used to keep the cell windows from condensing water vapor. A, B, C, D, and E are the positions of Chromel-Alumel thermocouples mounted to the cell wall to measure temperature.

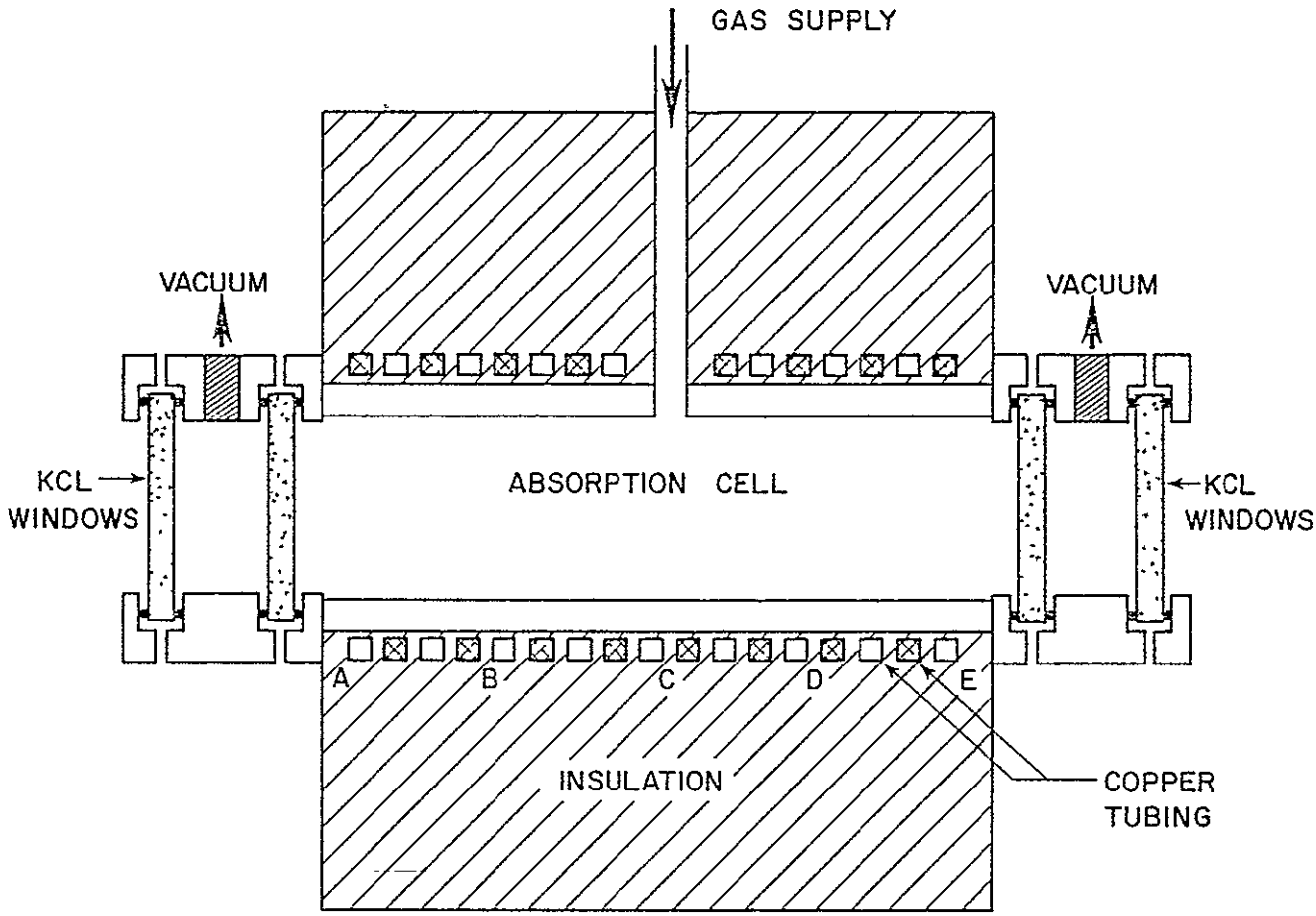

Figure 29. Electrical system for the temperature measurement. The numbers above the channel scanner represent the different channels of the scanner. Channel 0 was connected to an electronic manometer which measured the cell pressure. Channels 1 through 5 were connected to the thermocouples mounted along the absorption cell wall. The ratio from the boxcar was connected to channel 6, and channel 7 monitored the output of an ice bath thermocouple.

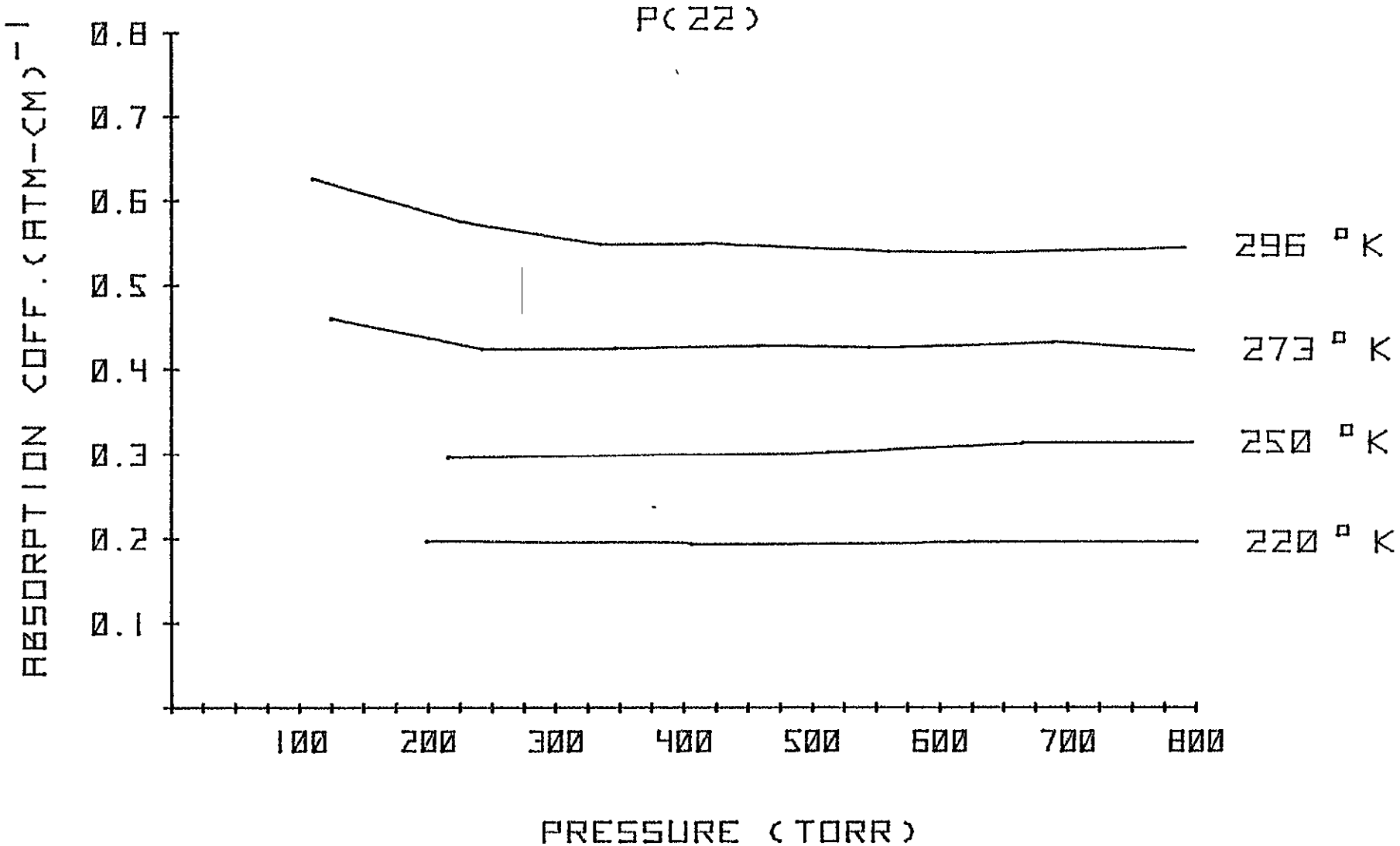

Figure 30. Pressure and temperature dependence of CFM-12 absorption coefficient for the P(22) CO_2 laser line. Note the pressure independence at each temperature studied. The absorption coefficients are not normalized for density changes at reduced temperatures.

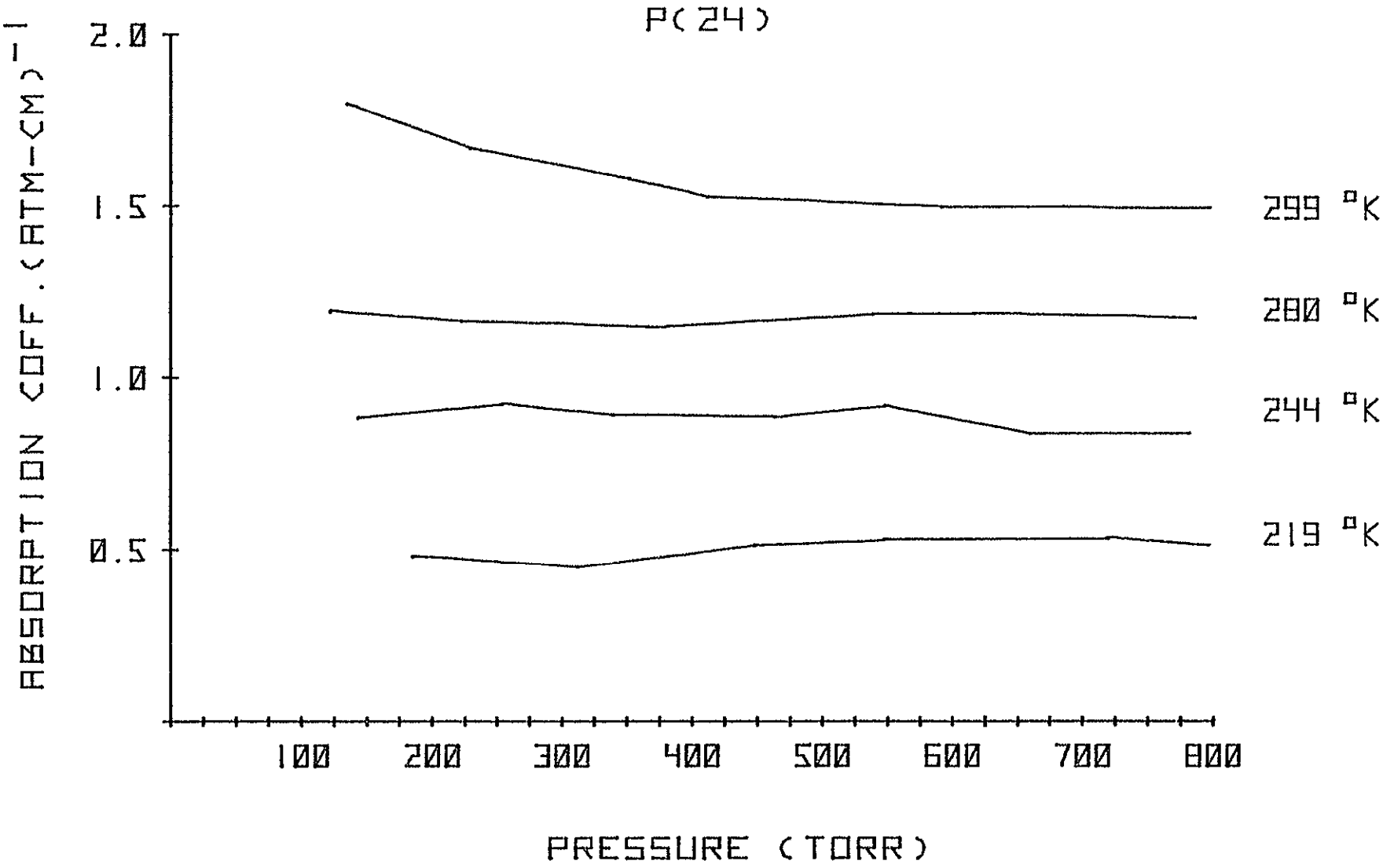

Figure 31. Pressure and temperature dependence of CFM-12 absorption coefficient for the P(24) CO_2 laser line. Note the pressure independence at each temperature studied. The absorption coefficients are not normalized for density changes at the reduced temperatures.

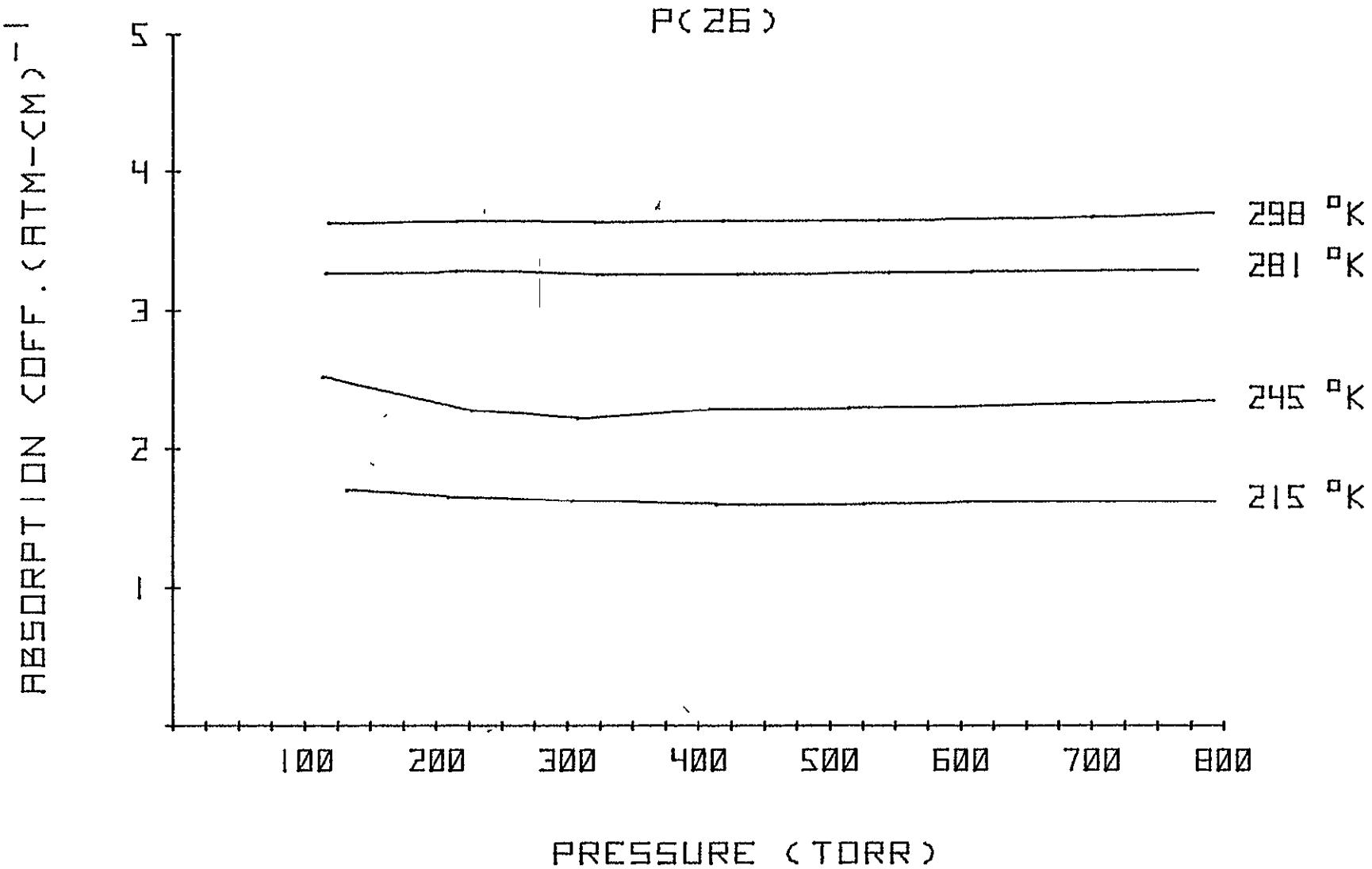

Figure 32. Pressure and temperature dependence of CFM-12 for the P(26) CO_2 laser line. Note the pressure independence at each temperature studied. The absorption coefficients are not normalized for density changes at the reduced temperatures.

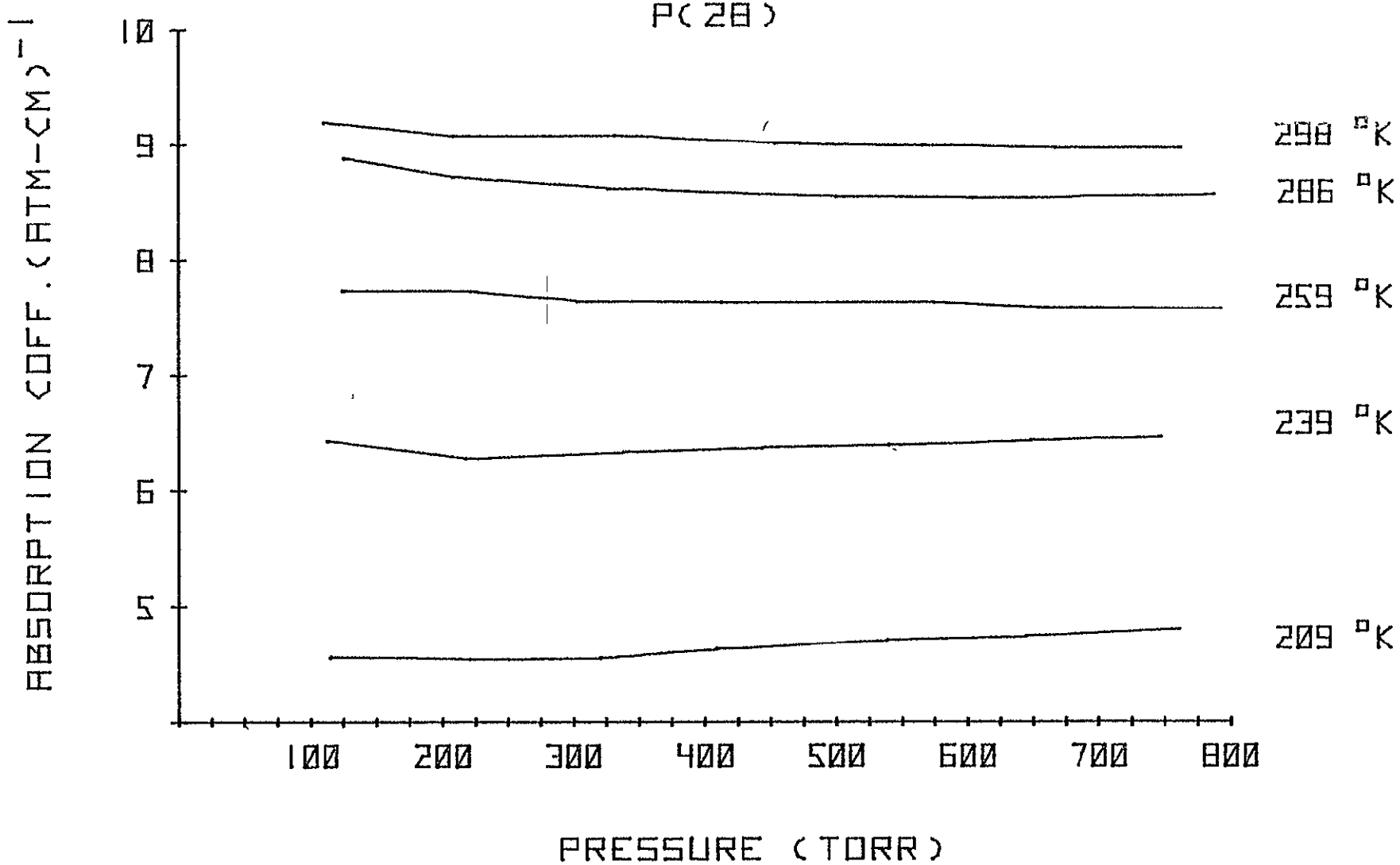

Figure 33. Pressure and temperature dependence of CFM-12 for the P(28) CO_2 laser line of the $00°1 - (10°0, 02°0)_I$ CO_2 band. Note the pressure independence at each temperature studied. The absorption coefficients are not normalized for density changes at reduced temperatures.

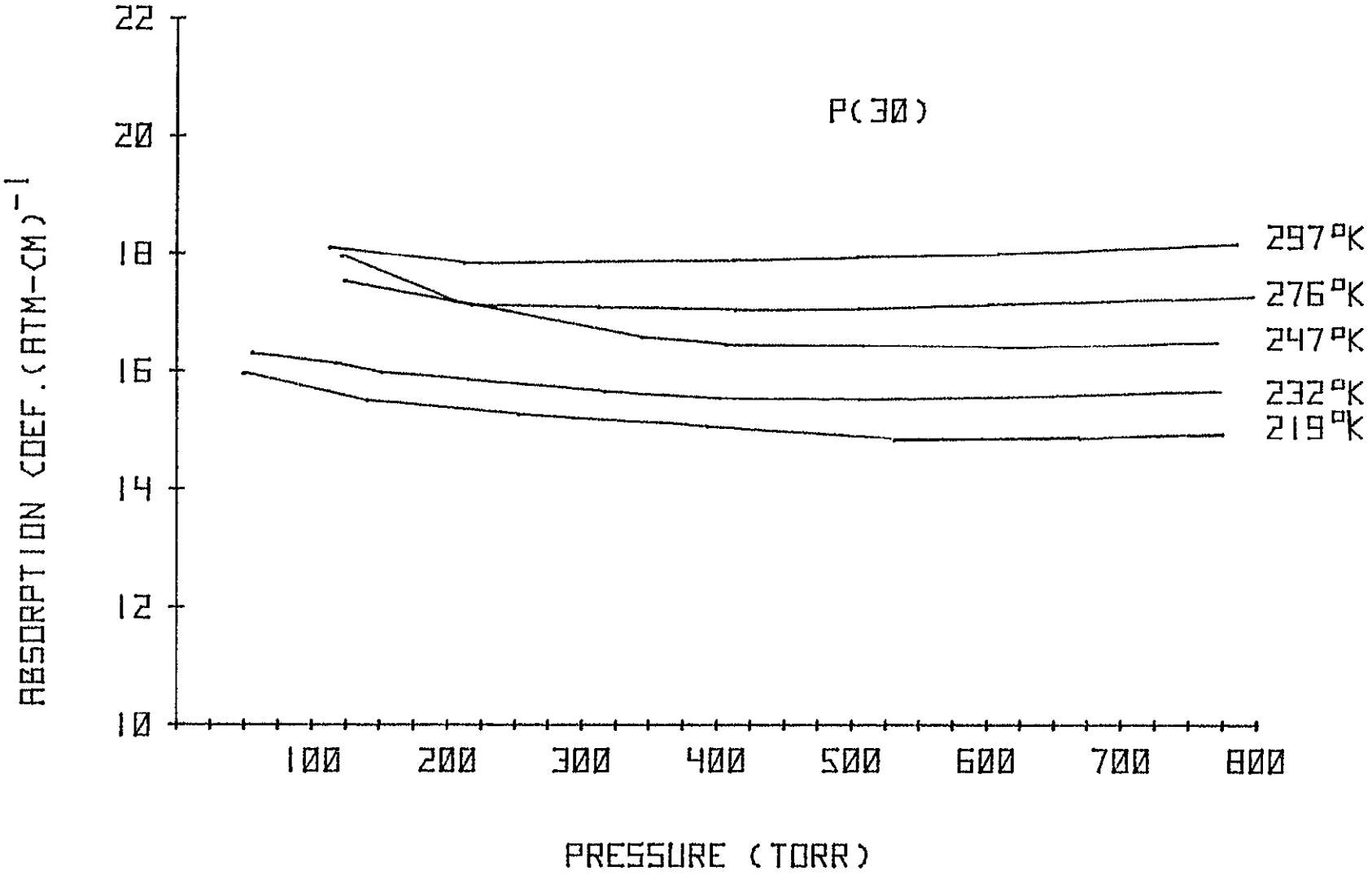

Figure 34. Pressure and temperature dependence of CFM-12 for the P(30) CO_2 laser line of the 00°1 - (10°0, 02°0)$_I$ CO_2 band. Note the pressure independence at each temperature studied. ^{I}The absorption coefficients are not normalized for density changes at reduced temperatures.

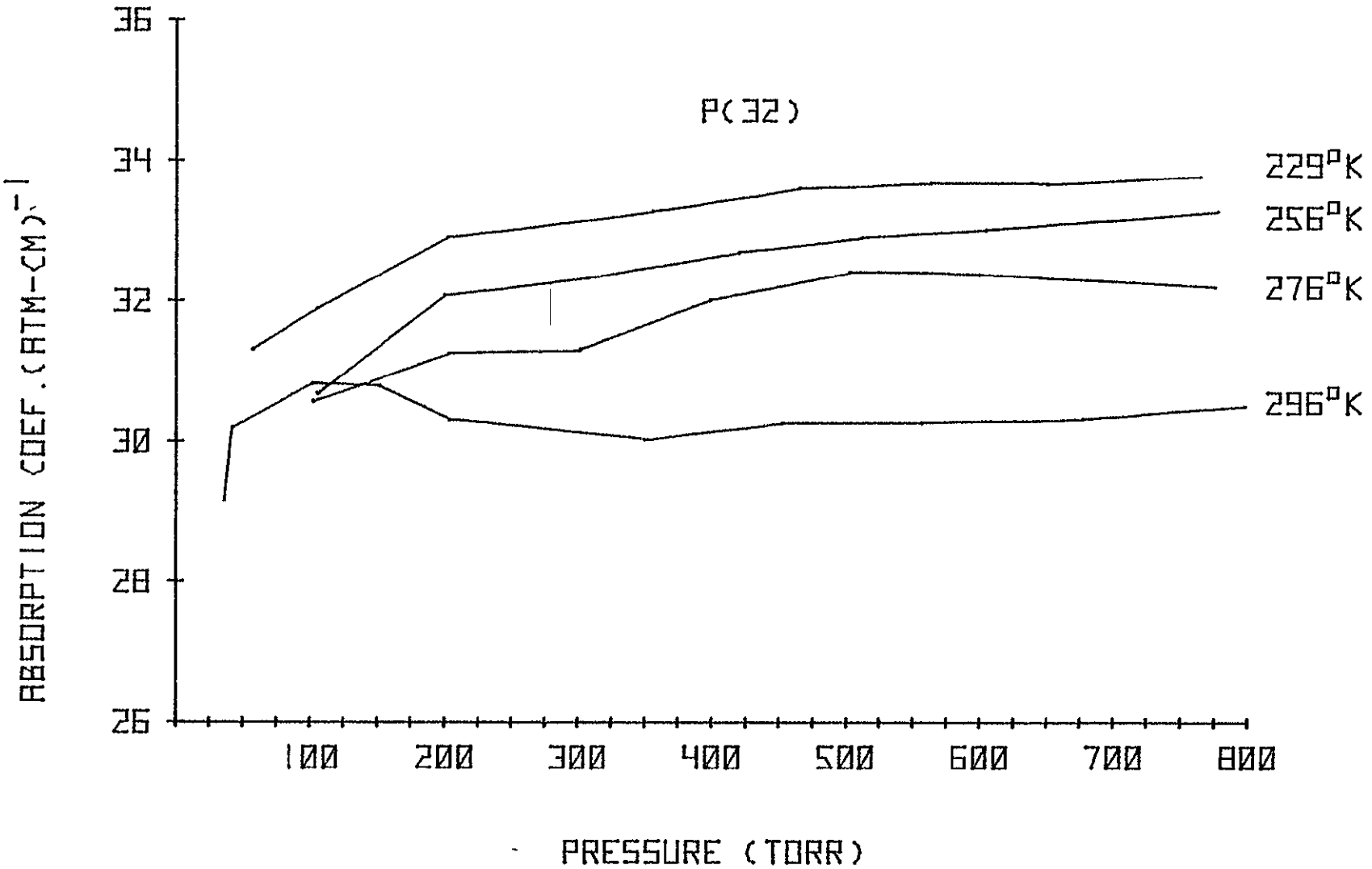

Figure 35. Pressure and temperature dependence of CFM-12 for the P(32) CO_2 laser line of the $00°1 - (10°0, 02°0)_I$ CO_2 band. Note the pressure independence at each temperature studied. The absorption coefficients are not normalized for density changes at reduced temperatures.

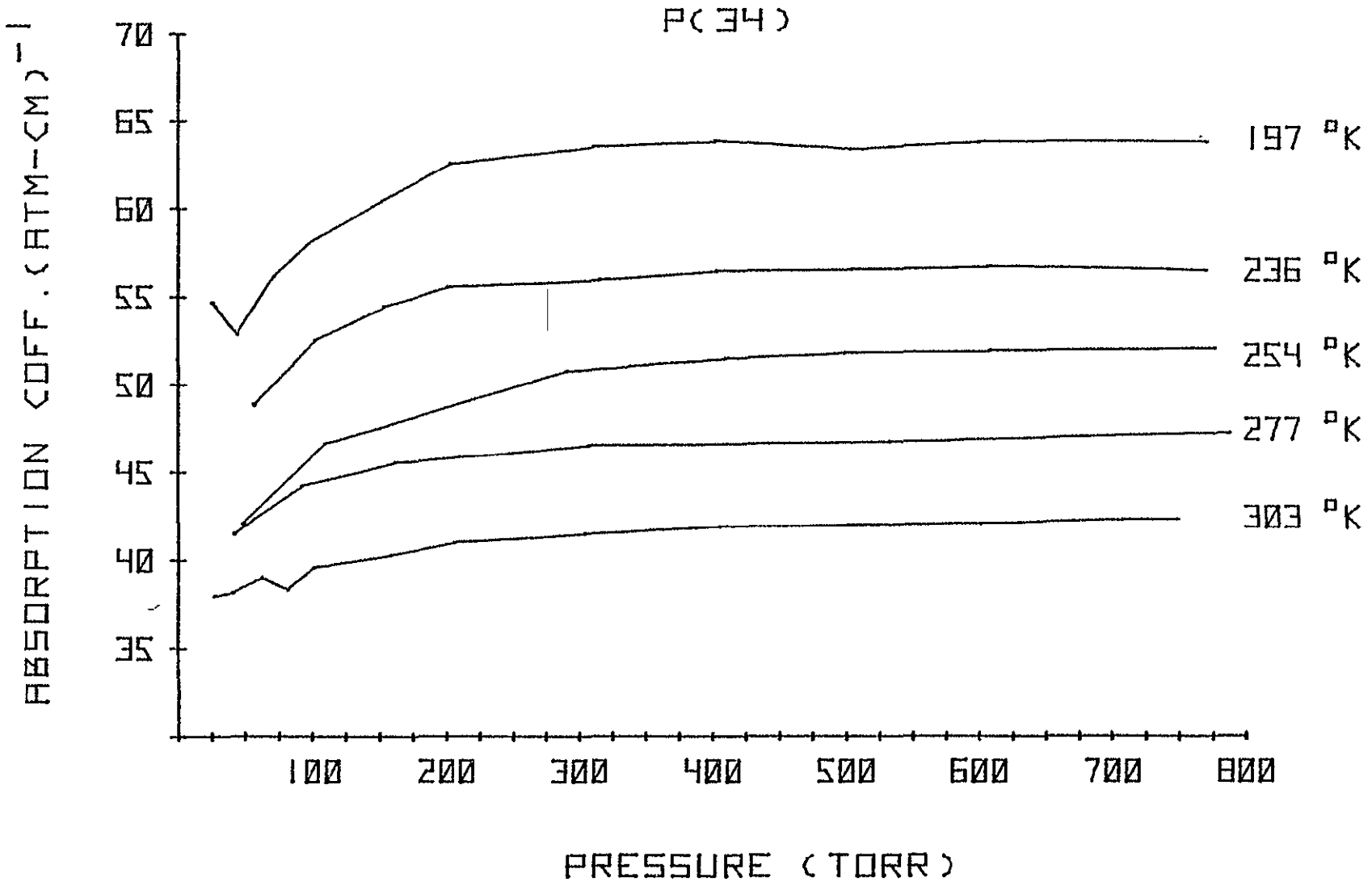

Figure 36. Pressure and temperature dependence of CFM-12 for the P(34) CO_2 laser line of the $00°1 - (10°0, 02°0)_I$ CO_2 band. Note the pressure independence at each temperature studied. The absorption coefficients are not normalized for density changes at reduced temperatures.

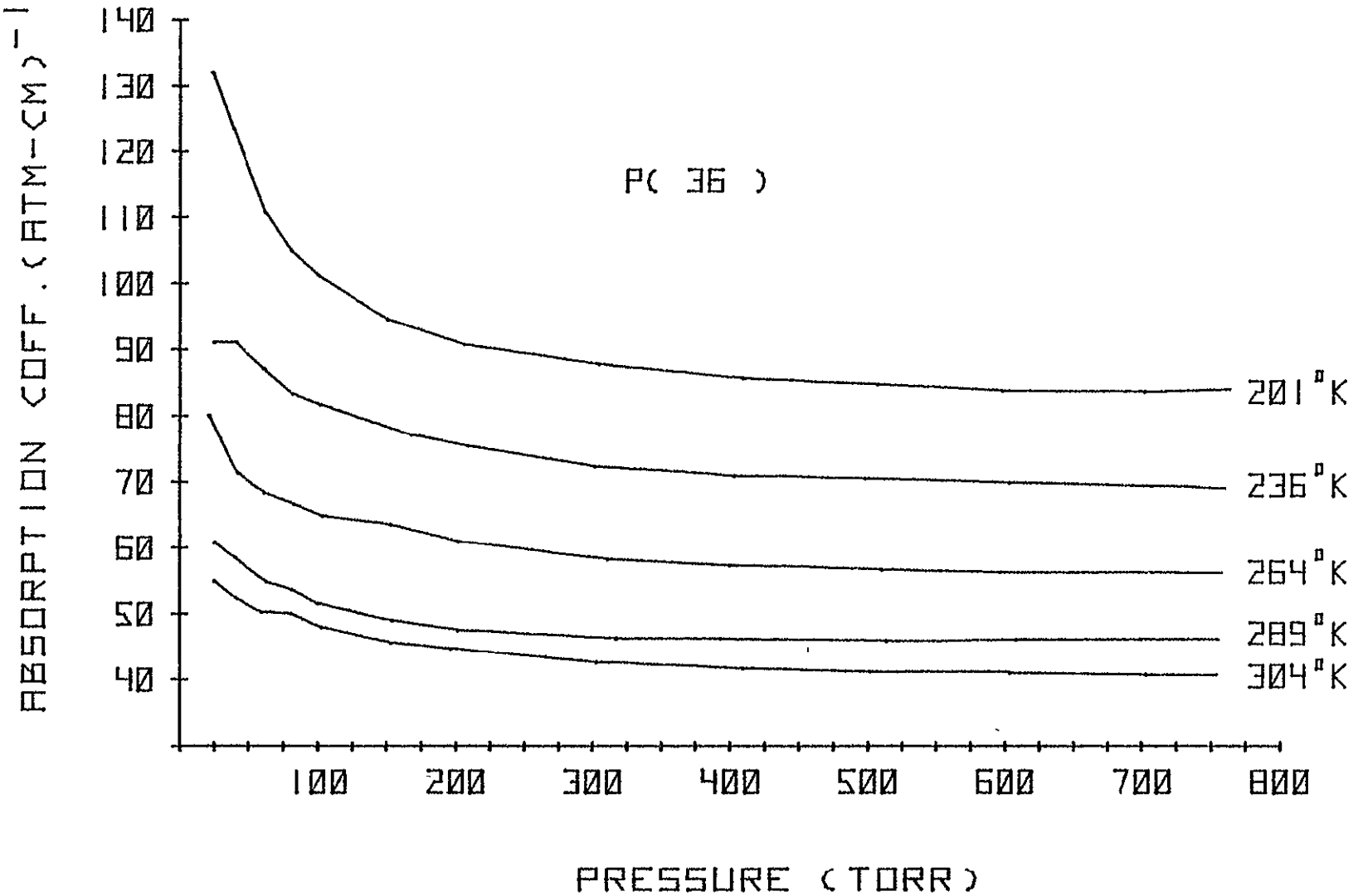

Figure 37. Pressure and temperature dependence of CFM-12 for the P(36) CO_2 laser line. Note the pressure independence does not occur except above 400 torr. The absorption coefficients are not normalized for density changes at the reduced temperatures.

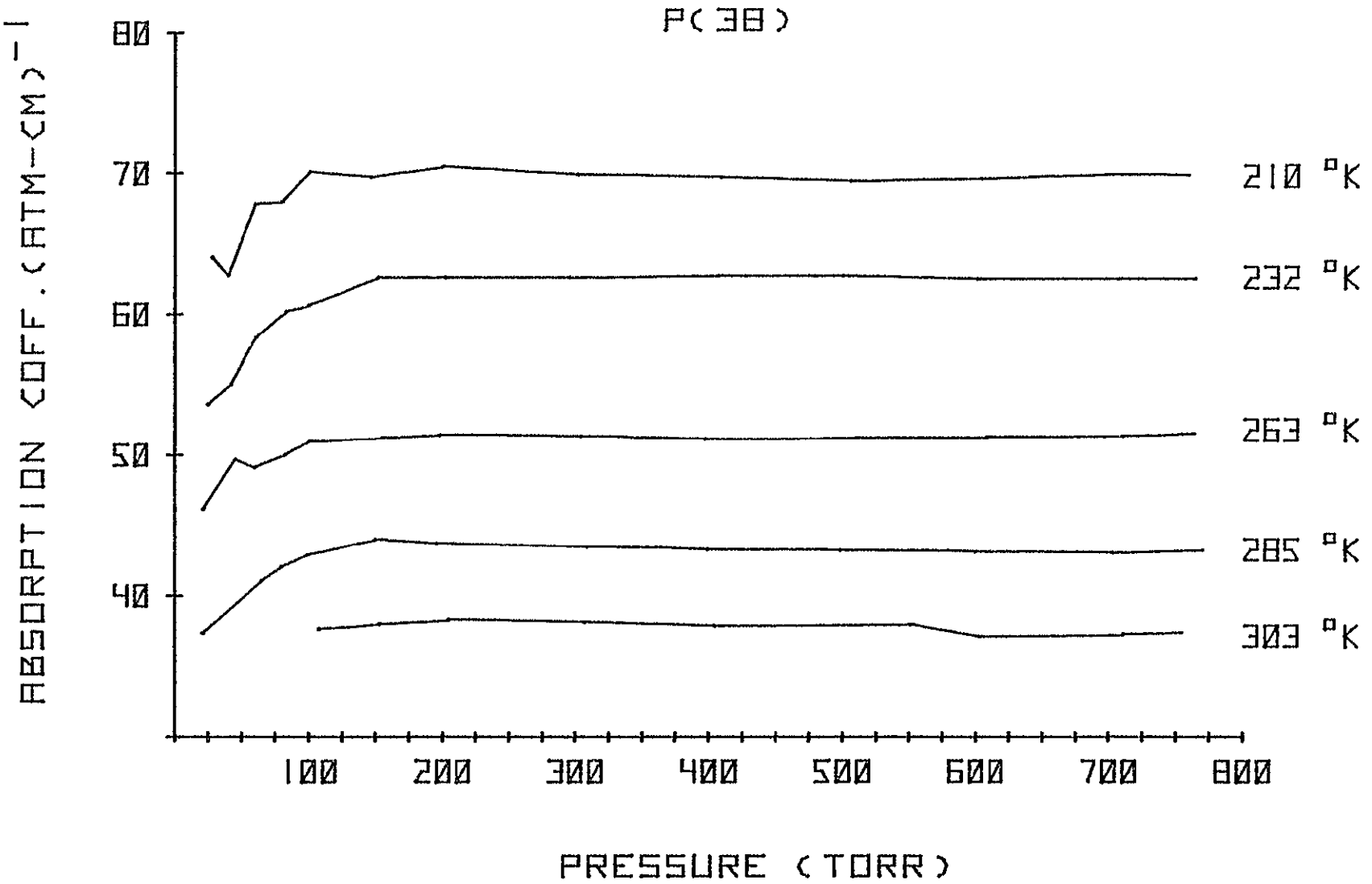

Figure 38. Pressure and temperature dependence of CFM-12 for the P(38) CO_2 laser line of the $00°1 - (10°0, 02°0)_I$ CO_2 band. Note the pressure independence at each temperature studied. The absorption coefficients are not normalized for density changes at reduced temperatures.

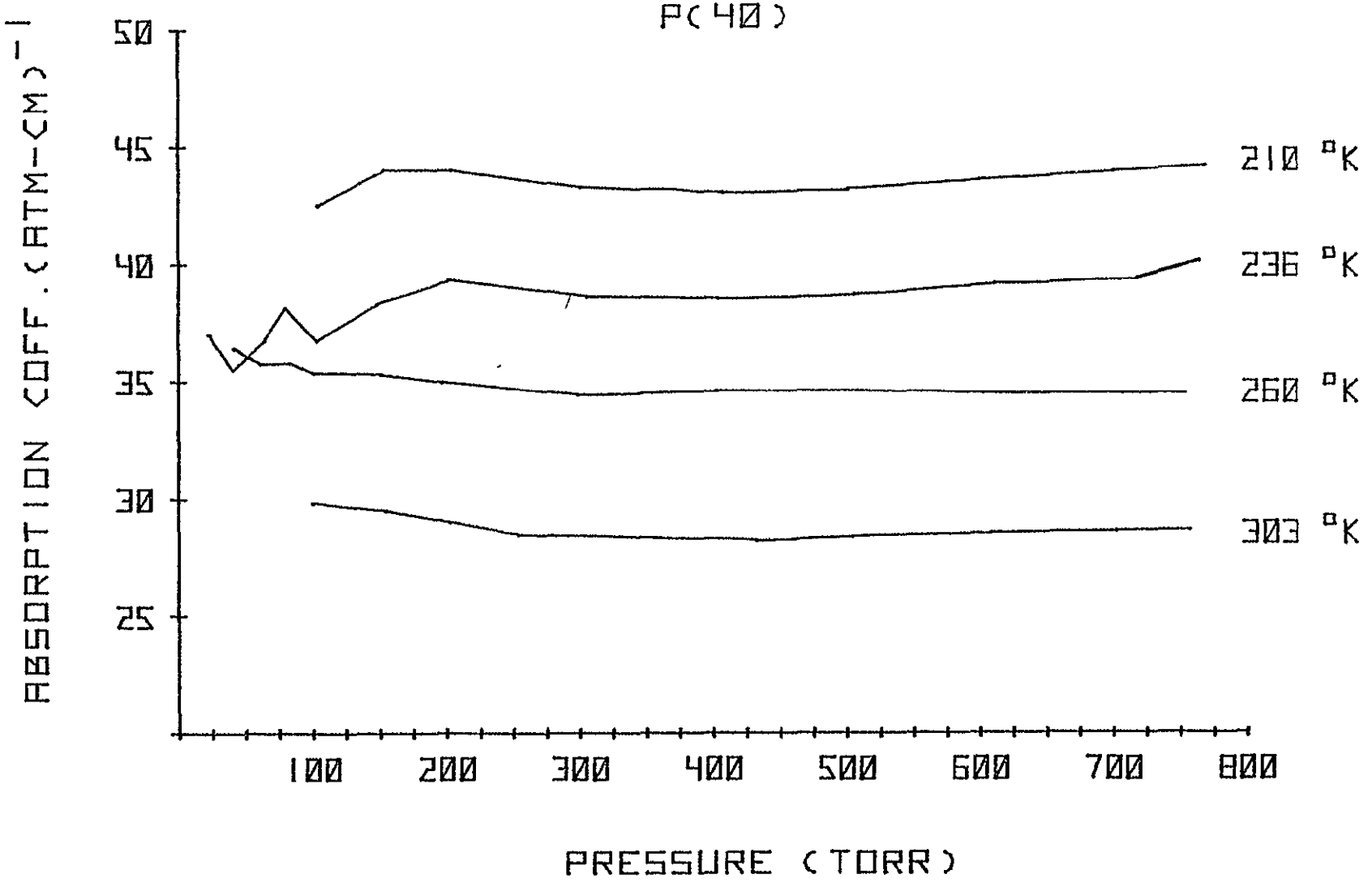

Figure 39. Pressure and temperature dependence of CFM-12 for the P(40) CO_2 laser line of the $00°1 - (10°0, 02°0)_I$ CO_2 band. Note the pressure independence at each temperature studied. The absorption coefficients are not normalized for density changes at reduced temperatures.

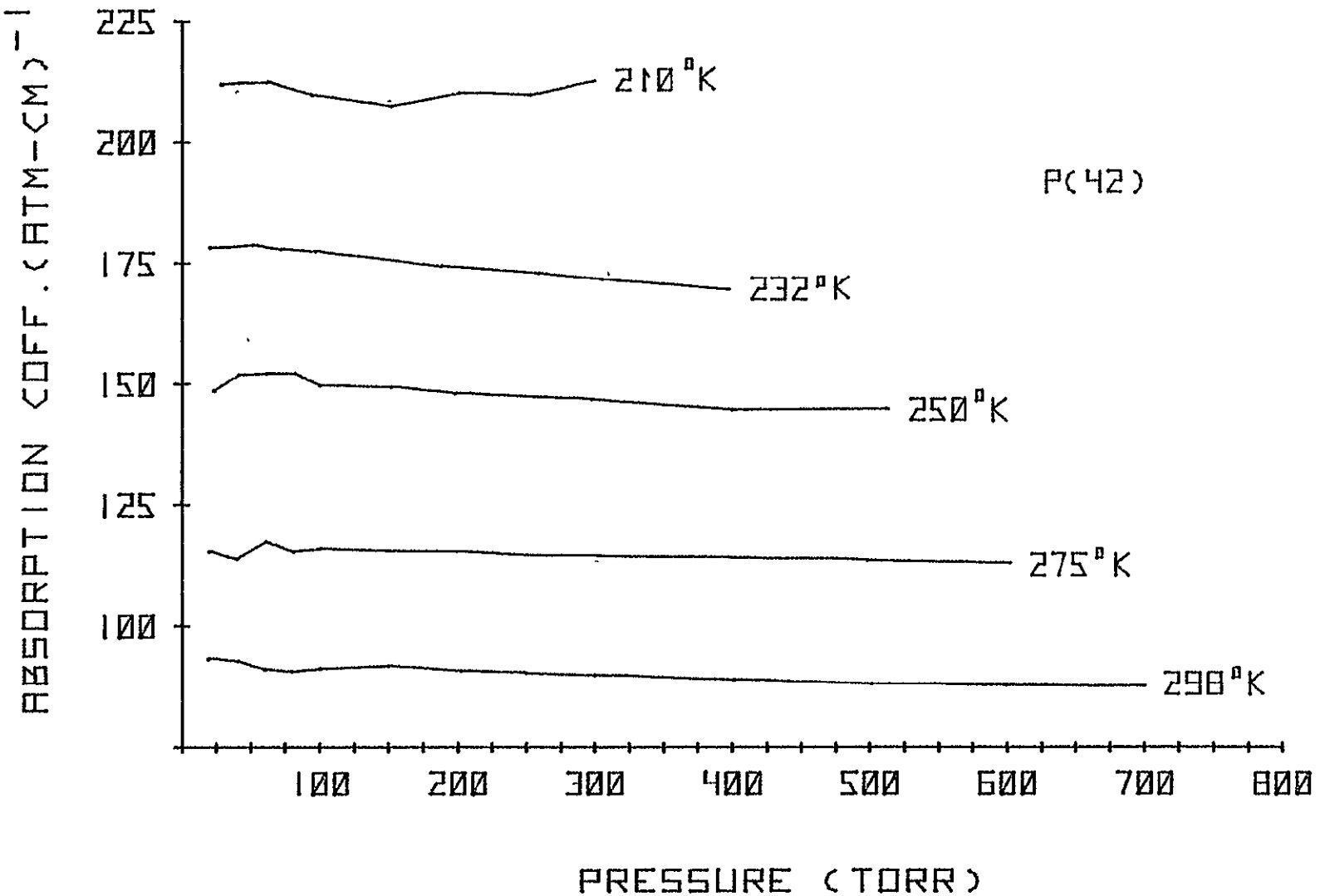

Figure 40. Pressure and temperature dependence of CFM-12 for the P(42) CO_2 laser line of the 00°1 - (10°0, 02°0)$_I$ CO_2 band. Note the pressure independence at each temperature studied. The absorption coefficients are not normalized for density changes at reduced temperatures.

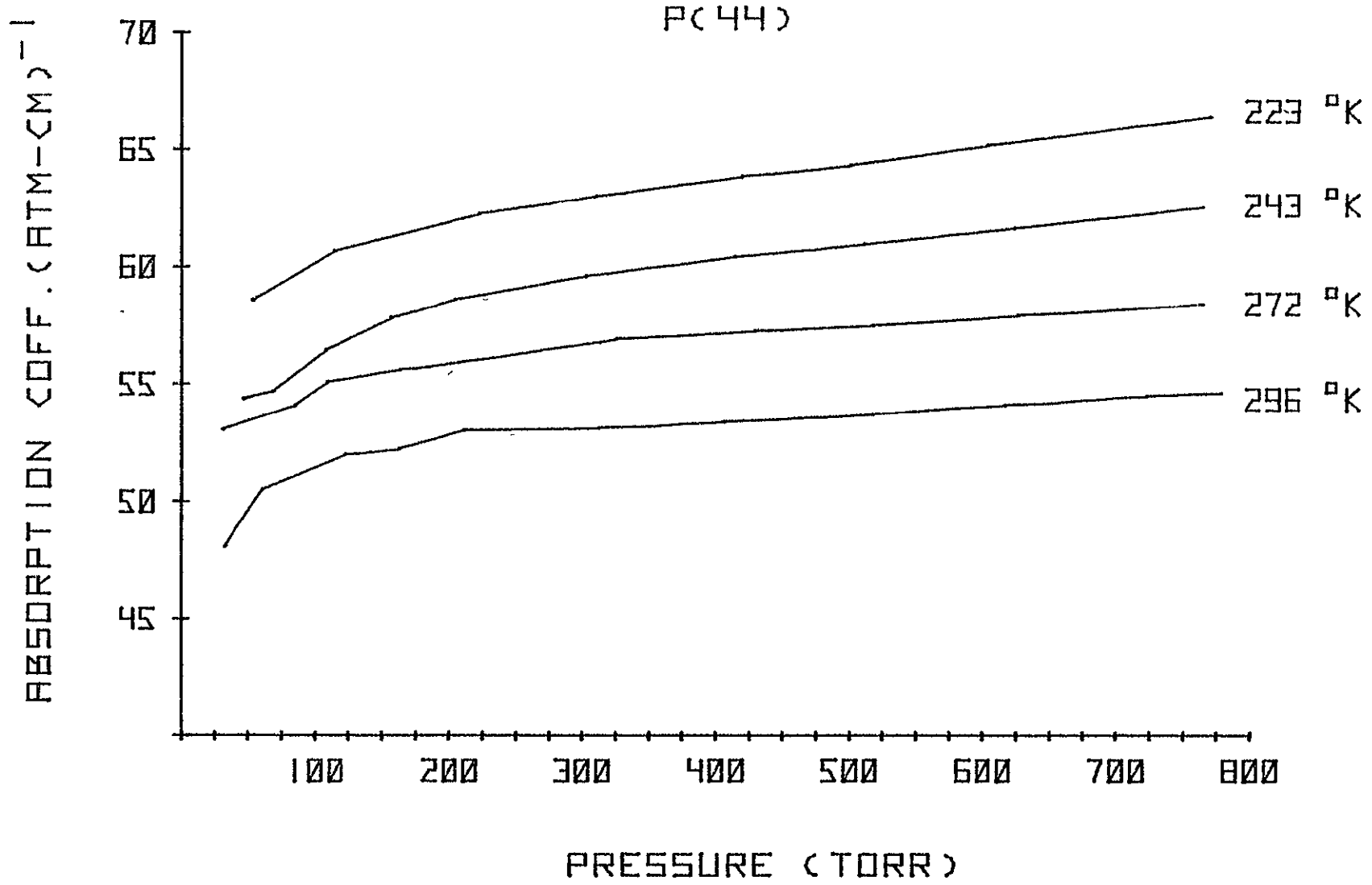

Figure 41. Pressure and temperature dependence of CFM-12 for the P(44) CO_2 laser line of the $00^{\circ}1 - (10^{\circ}0, 02^{\circ}0)_I$ CO_2 band. Note the pressure independence at each temperature studied. The absorption coefficients are not normalized for density changes at reduced temperatures.

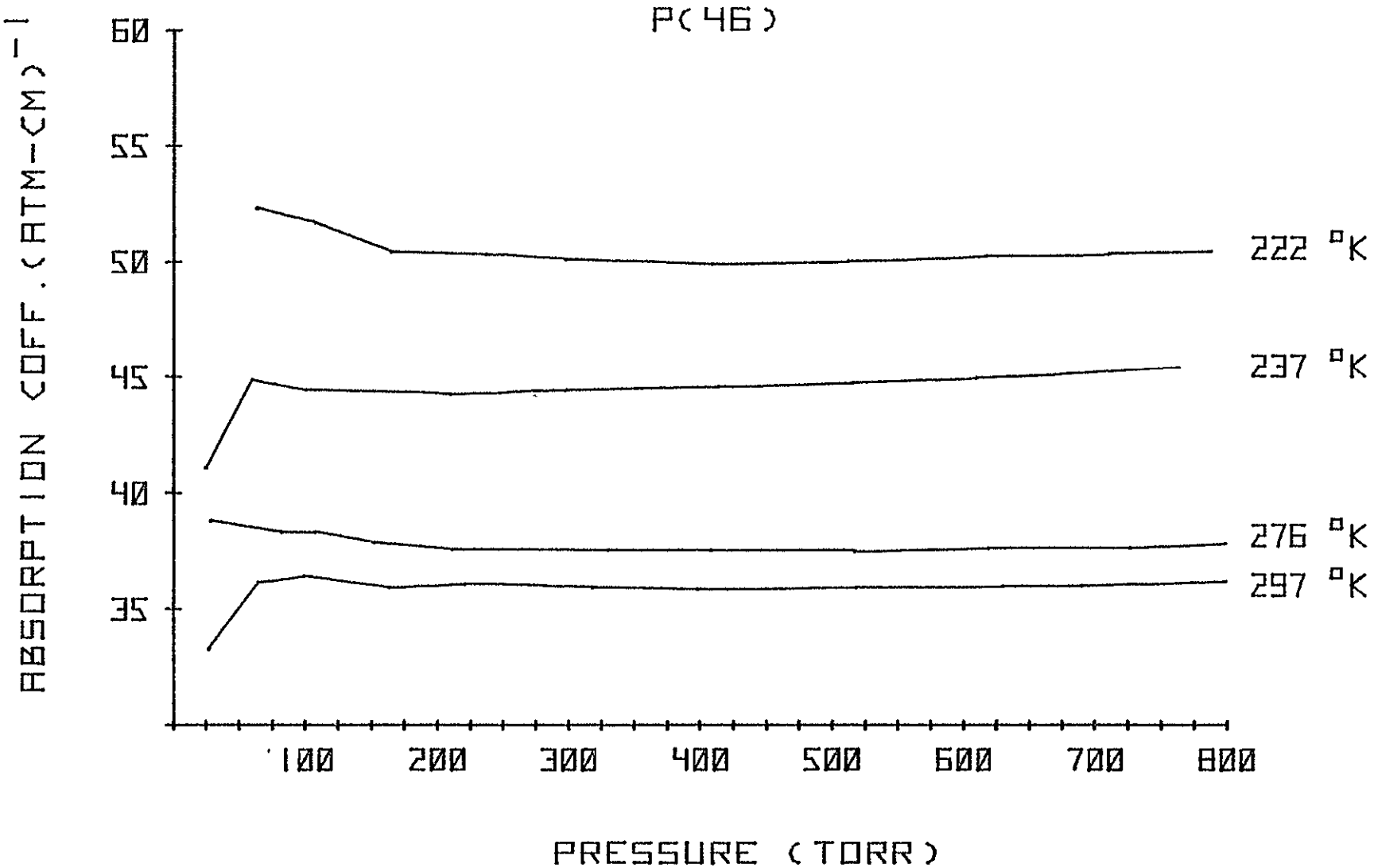

Figure 42. Pressure and temperature dependence of CFM-12 for the P(46) CO_2 laser line of the $00°1 - (10°0, 02°0)_I$ CO_2 band. Note the pressure independence at each temperature studied. The absorption coefficients are not normalized for density changes at reduced temperatures.

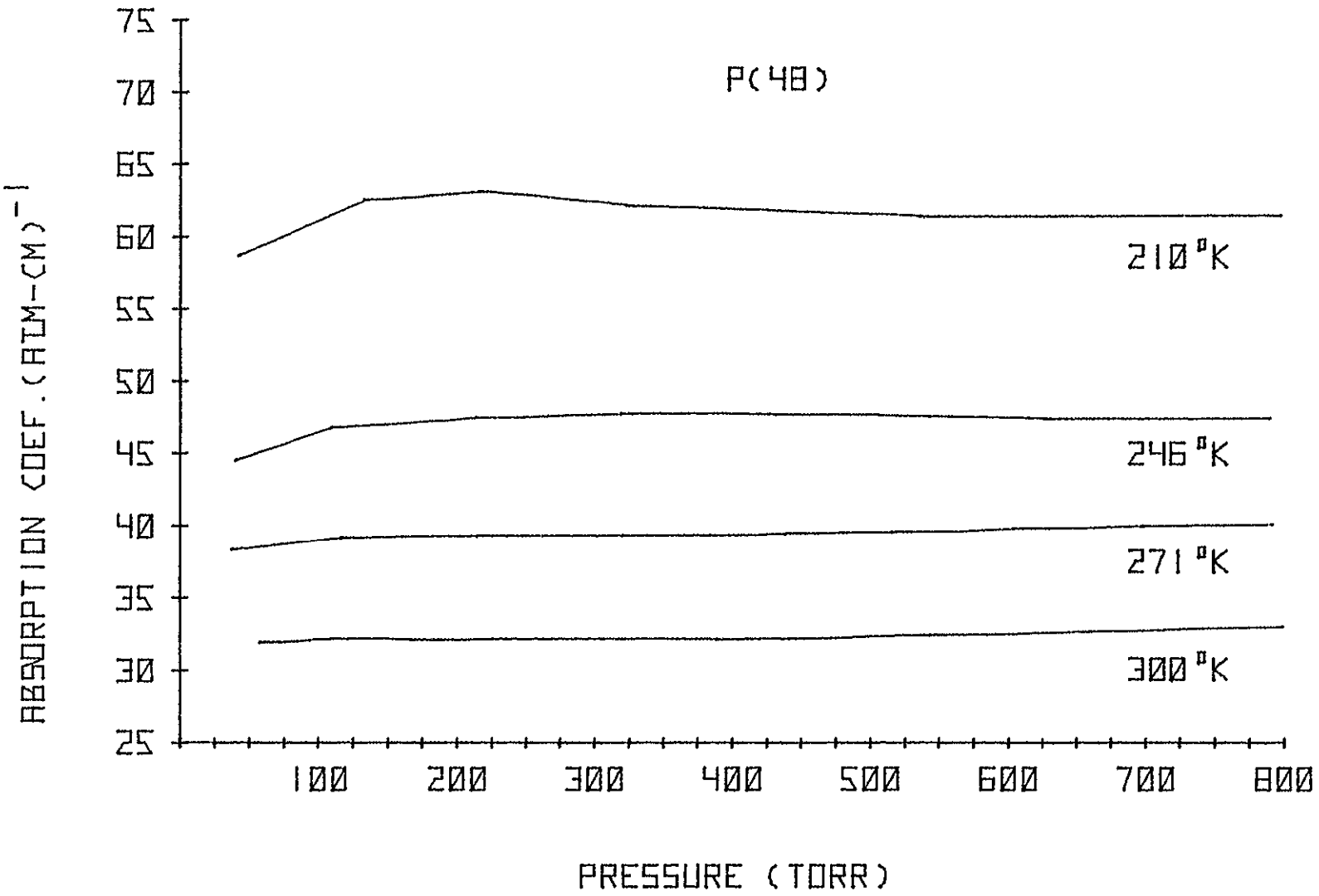

Figure 43. Pressure and temperature dependence of CFM-12 for the P(48) CO_2 laser line of the $00°1 - (10°0, 02°0)_I$ CO_2 band. Note the pressure independence at each temperature studied. The absorption coefficients are not normalized for density changes at reduced temperatures.

REFERENCES

1. Abrams, R.L.: Appl. Phys. Let., 25, 304, 1974.

2. Bradford, C.M.; Murcray, F.H.; van Allen, J.W.; Brooks, J.N.; Murcray, D.G.; and Goldman, A.: Ground Level Detection and Feasibility for Monitoring of Several Trace Atmospheric Constituents by High Resolution Infrared Spectroscopy. Geophys. Res. Let., 3, 7, 387-390, July 1976.

3. Goldman, A.; Bonomo, F.S.; and Murcray, D.G.: Statistical-Band-Model Analysis and Integrated Intensity for the 10.8 Micron Band of CF_2CL_2. Geophys. Res. Let., 3, 309-312, June 1976.

4. Herdt, L.E.; Lueb, R.; Pollock, W.; and Ehhalt, D.H.: Stratospheric Profiles of CCL_3F and CCL_2F_2. Geophys. Res. Let., 2, 445, 1975.

5. Hinkley, E.D.; Ku, R.T.; Nill, K.W.; and Butler, J.F.: Long-Path Monitoring Advanced Instrumentation With a Tunable Diode Laser. Applied Optics, 15, 7, 1653-1655, July 1976.

6. Lovelock, J.E.: Atmospheric Halocarbons and Stratospheric Ozone. Nature, 252, 292-294, 1974.

7. Menzies, Robert T.: Ozone Spectroscopy With a CO_2 Waveguide Laser. Applied Optics, 15, 11, 2597-2599, 1976.

8. Molina, M.J.; and Rowland, F.S.: Stratospheric Sink for Chlorofluoromethanes - Chlorine Atom Catalyzed Destruction of Ozone. Nature, 249, 810-812, 1974.

9. Murcray, D.G.; Bonomo, F.S.; Brooks, J.N.; Goldman, A.; Murcray, F.H.; and Williams, W.J.: Detection of Fluoro-carbons in the Stratosphere. Geophys. Res. Let., 2, 3, March 1975.

10. Peyton, B.J.; Lange, R.A.; Savage, M.G.; Seals, R.K.; and Allario, F.: Infrared Heterodyne Spectrometer Measurements of Vertical Profile of Tropospheric Ammonia and Ozone. AIAA 15th Aerospace Sciences Meeting, Los Angeles, CA, January 24-26, 1977.

11. Schnell, W.; and Fischer, G.: Detection of Air Pollutants With a Tunable CO_2 Laser. Zeitschr. Angew. Math. Phys., 26, 133, 1975, and private communication.

12. Seals, R.K.; and Peyton, B.J.: Remote Sensing of Atmospheric Pollutant Gases Using an Infrared Heterodyne Spectrometer. Proceedings of the International Conference on Environmental Sensing and Assessment, Las Vegas, NV, September 1975, 1, 10-4.